
Transports across the 2002 Greenland-Portugal Ovide section and comparison with 1997

P. Lherminier¹, H. Mercier¹, C. Gourcuff¹, M. Alvarez²,
S. Bacon³ and C. Kermabon¹

1 Laboratoire de Physique des Océans (LPO), Ifremer, Plouzané, France

2 Instituto de Investigaciones Marinas (CSIC), Vigo, Spain. Now at Facultade de Ciencias, Univ. Vigo, Campus Lagoas Marcosende, s/n 36200, Vigo, Spain

3 National Oceanographic Centre (NOC), Southampton, UK

Abstract:

The first Ovide cruise occurred in June–July 2002 on R/V *Thalassa* between Greenland and Portugal. The absolute transports across the Ovide line are estimated using a box inverse model constrained by direct acoustic Doppler current profiler velocity measurements and by an overall mass balance (± 3 Sv, where $1 \text{ Sv} = 10^6 \text{ m}^3 \text{ s}^{-1}$) across the section. Main currents are studied and compared to the results of the similar Fourex section performed in August 1997 and revisited here. The meridional overturning cell (MOC) is estimated in two different ways, both leading to a significantly lower value in June 2002 than in August 1997, consistent with the relative strength of the main components of the MOC (North Atlantic Current and deep western boundary current). It has been found that the MOC calculated on density levels is more robust and meaningful than when calculated on depth levels, and it is found to be 16.9 ± 1.0 Sv in 2002 versus 19.2 ± 0.9 Sv in 1997. The 2002 heat transport of $0.44 \pm 0.04 \times 10^{15}$ W is also significantly different from the $0.66 \pm 0.05 \times 10^{15}$ W found in 1997, but it is consistent with the much weaker integrated warm water transport across the section than in 1997.

Keywords: North Atlantic circulation; meridional overturning cell; hydrographic section

Transports across the 2002 Greenland-Portugal Ovide Section and Comparison with 1997

P. Lherminier,¹ H. Mercier,¹ C. Gourcuff,¹ M. Alvarez,² S. Bacon³ and C. Kermabon,¹

Abstract.

The first Ovide cruise occurred in June-July 2002 on R/V Thalassa between Greenland and Portugal. The absolute transports across the Ovide line are estimated using a box inverse model constrained by the direct acoustic Doppler current profiler velocity measurements and by an overall mass balance (± 3 Sv, where $1 \text{ Sv} = 10^6 \text{ m}^3 \text{ s}^{-1}$) across the section. Main currents are studied, and compared to the results of the similar Fourex section performed in August 1997 and revisited here. The Meridional Overturning Cell (MOC) is estimated in two different ways, both leading to a significantly lower value in June 2002 than in August 1997, consistent with the relative strength of the main components of the MOC (North Atlantic Current and Deep Western Boundary Current). It has been found that the MOC calculated on density levels is more robust and meaningful than when calculated on depth levels, and is found to be 16.9 ± 1.0 Sv in 2002, versus 19.2 ± 0.9 Sv in 1997. The 2002 heat transport of $0.44 \pm 0.04 \times 10^{15}$ W is also significantly different from the $0.66 \pm 0.05 \times 10^{15}$ W found in 1997, but it is consistent with the much weaker integrated warm water transport across the section than in 1997.

1. Introduction

The upper limb of the Meridional Overturning Cell (MOC) in the North Atlantic carries warm, salty water which is progressively cooled and transformed into subpolar mode water and intermediate and deep waters by winter convection in the Labrador, Irminger Sea and Greenland Sea as well as by transformation on the continental shelves. The lower limb of the MOC carries these cold waters southward. They are modified by entrainment of warmer waters when crossing the bathymetric sills separating the basins. There is also a return surface branch carrying fresh, cold water originating in the Arctic. This MOC is associated with northward heat transport in the North Atlantic and its variability could be related to European climate change.

The warm, salty water is transported in the North Atlantic Current (NAC) toward the subpolar seas. Its variability has been indirectly studied through observations by *Bryden et al.* [2005], who find in the subtropics a decrease of about 6 Sv ($1 \text{ Sv} = 10^6 \text{ m}^3 \text{ s}^{-1}$) in the transport of the lower component of the North Atlantic Deep Water since 1957, consistent with the baroclinic Deep Western Boundary Current reduction of about 5 Sv seen after about 1990 in *Bacon* [1998a].

In *Bryden et al.* [2005], this long-term variability is compensated by a stronger southward thermocline flow, thus leading to a plausible decrease in the NAC net northward transport. However, these changes are not easily captured with existing observations north of 50°N when one considers the strength of the monthly to interannual variability and the complex relation between the very strong Subtropical Gyre intensity and the eddy rich and relatively weak NAC at this latitude. *Curry and McCartney* [2001] find that at higher latitudes, the low-frequency NAC variability is relatively well captured by a transport index, based on potential energy anomaly between the Labrador Basin and Bermuda. This index relates to the combined Subtropical

and Subpolar Gyre transport variability responding to the North Atlantic Oscillation (NAO) on the decadal timescale, and shows a maximum in the early 1990s after a minimum in the 1960s. The authors emphasize the strong non-linearities that lead to important interannual variability. Following the same general idea, *Häkkinen and Rhines* [2004] compute a Subpolar Gyre index and exhibit a weakening of the Subpolar Gyre surface circulation in the late 1990s, found to be the low-frequency response to the NAO and consistent with *Flatau et al.* [2003]. *Hátún et al.* [2005] correlate this circulation weakening to the North Atlantic Current westward shift (also shown by *Bersch* [2002]) and salinity increase. However, it is not clear that the integrated transport of the NAC shows a correlated variability.

Interannual variability of overflow transport and properties is documented by *Macrander et al.* [2005] in the Denmark Strait and *Hansen and Østerhus* [2006] in the Faroe Bank Channel. They both show that although the monthly to interannual variability can reach 1 Sv, there is no observable decadal trend. However, hydrological properties of the overflows show an overall freshening that is reported in *Dickson et al.* [2002] along with all the components of the North Atlantic Deep Water.

¹Laboratoire de Physique des Océans (LPO), Ifremer, Plouzané, France

²Instituto de Investigaciones Marinas (CSIC), Vigo, Spain. Now at Facultad de Ciencias, Univ. Vigo, Campus Lagoas Marcosende, s/n 36200, Vigo, Spain

³National Oceanographic Centre (NOC), Southampton, UK

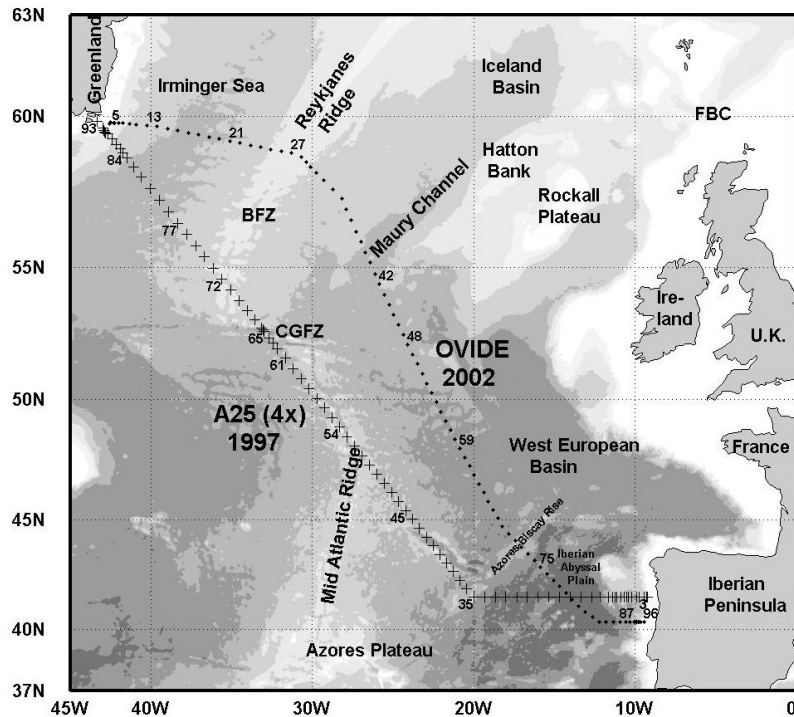


Figure 1. Ovide (squares) and Fourex (crosses) hydrological station locations plotted on bathymetry (500m intervals). CGFZ: Charlie-Gibbs Fracture Zone; BFZ: Bight Fracture Zone. FBC: Faroe-Bank Channel.

The MOC variability is the result of the variability of all the above components. It has been studied mainly in models, where it is generally computed as the maximum of the vertical stream function annual mean. Using hydrographic data, *Koltermann et al.* [1999] and *Bryden et al.* [2005] presented such analyses based on repeat hydrographic sections (at 48°N and 25°N respectively) that intersect the main components of the MOC, and both observed an MOC variability. The Ovide (Observatoire de la Variabilité Interannuelle à DEcennale) project aims to repeat a trans-oceanic hydrographic section from Greenland to Portugal every other year (Figure 1). It is part of the CLIVAR and CARBOOCEAN international programs that are focused on ocean climate variability. The chosen section crosses the main currents implicated in the North Atlantic MOC, and is close to the A25 section (“Fourex”) of the World Ocean Circulation Experiment performed in 1997. The goal is to contribute to the monitoring of the inter-annual variability of the water masses as well as the variability of the mass, heat, and tracer transports in the northern

North Atlantic Ocean, based on thermal wind equations and mass balance, but also on direct current measurements along the section.

We present an analysis of the Ovide first realization that was carried out in June–July 2002. Results from the 1997 Fourex section discussed in *Álvarez et al.* [2004] have been revisited with the same method. Main transports of August 1997 and June–July 2002 could then be consistently compared. A discussion of the estimation and variability of the MOC in these data follows, leading to the calculation of the MOC in potential density coordinates (MOC_{σ}) that is likely to be the most significant index on such a section for water mass transformation north of the section and for the MOC.

2. Data Set

2.1. CTD Data

The Ovide 2002 cruise was carried out on the French R/V *Thalassa*. The hydrographic section started on 18 June 2002 off Greenland and ended on 10 July 2002 off Portugal. A total of 104 hydrographic stations were carried out. Only 90 stations (numbers 6 to 96), which

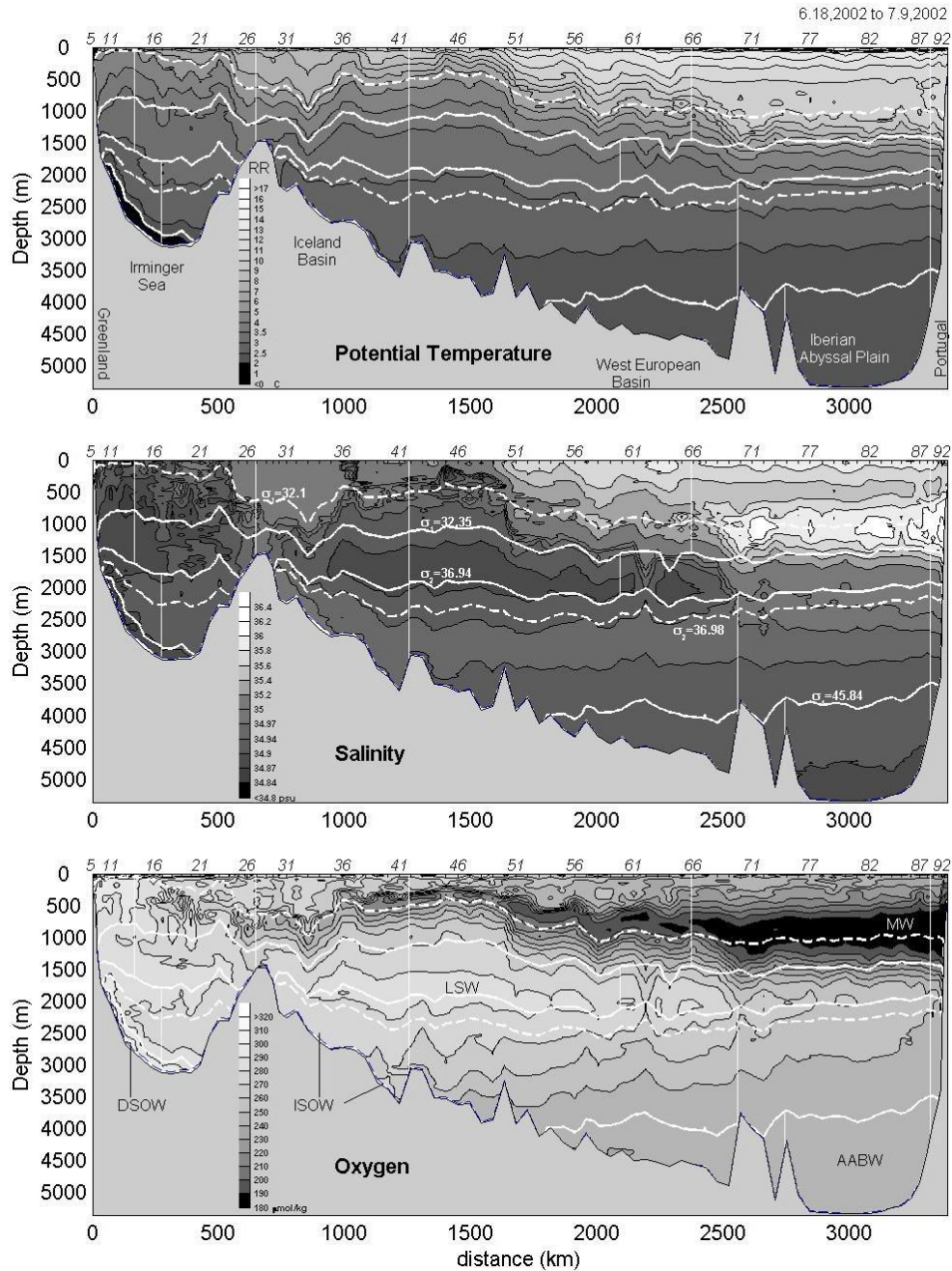


Figure 2. Section of temperature, salinity and oxygen along the Ovide line, from Greenland (left) to Portugal (right). Isopycnals are drawn in white; continuous lines for $\sigma_1 = 32.35$, $\sigma_2 = 36.94$ and $\sigma_4 = 45.84$ and dashed lines for $\sigma_1 = 32.1$ and $\sigma_2 = 36.98$. Vertical white lines delimit the main regions of the section shown on Figure 10. Water masses discussed in the text are shown on the bottom panel: Denmark Strait Overflow Water (DSOW), Iceland-Scotland Overflow Water (ISOW), Labrador Sea Water (LSW), Antarctic Bottom Water (AABW) and Mediterranean Water (MW).

form the coast to coast section, are used in this work (Figure 1). At the time R/V *Thalassa* arrived at the tip of Greenland, the shelf was covered with ice, preventing any measurement to be carried out inshore of the 200 m bathymetric contour. The section was interrupted at station 72 for recovering moorings. It was resumed 4 days later at exactly the same location (sta-

tion 73). Since θ -S properties and currents measured at stations 72 and 73 were acceptably similar, we chose to ignore the latter in our analysis. At the end of the section, measurements were carried out on the Portugal Shelf.

At each station, measurements of temperature, salinity and dissolved oxygen concentration as a function of pressure were obtained using a Neil Brown Mark III

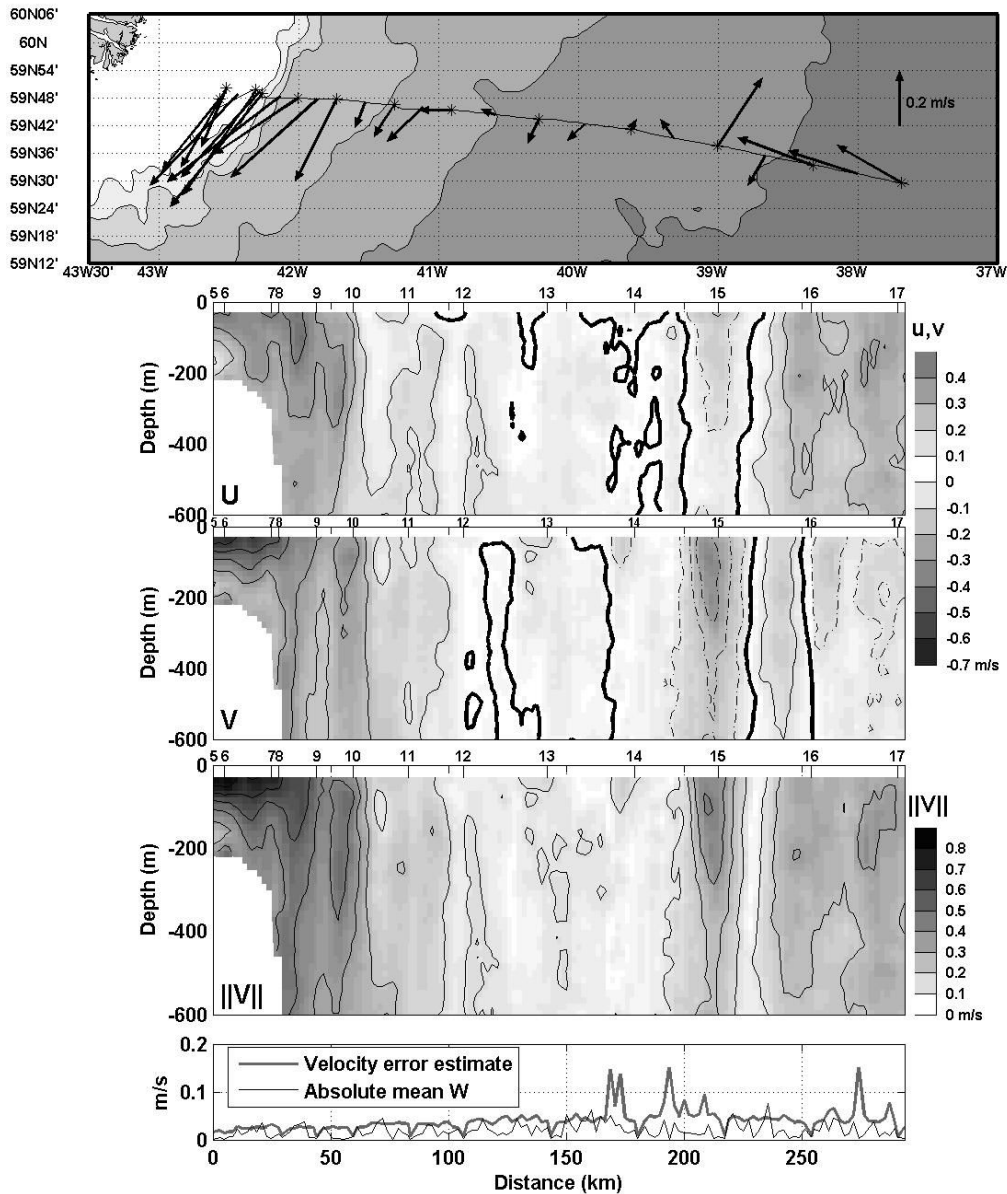


Figure 3. Currents measured by the SADC. The ship route of the northern part of the section is shown on the first panel, on top of bathymetry (500m intervals). The south tip of Greenland (Cape Farewell) is visible. Stars indicate stations and vectors are local subsurface velocities, averaged between 100 and 200m and between stations (or for station duration). The three central plots present the zonal (U , positive eastward), meridional (V , positive northward) and absolute ($\|V\|$) velocities as a function of distance (from station 5) and depth. Contours are plotted every 0.1 m s^{-1} ; they are dashed for positive values (for U and V only) and bold for the 0 contour. The white patch indicates the seafloor. The bottom plot presents an error estimate of the 20-ensemble mean velocity and an average of the vertical velocity, both between 100 and 400m.

CTDO₂ probe. The rosette was equipped with 28 8-liter bottles. Seawater samples were analysed on board R/V *Thalassa* to determine salinity and dissolved oxygen concentration - for CTDO₂ calibration purpose - as well as nutrients, CFCs, pH and alkalinity. The CTDO₂ measurement accuracies are thought to be better than 1 db for pressure, 0.002°C for temperature, 0.003 for salinity and $1 \mu\text{mol kg}^{-1}$ for dissolved oxygen [Billant

et al., 2004]. For further reference, the vertical sections of properties (θ , S , O_2) are shown in Figure 2.

2.2. SADC Data

Velocity measurements between 32 m and 600 m were obtained using R/V *Thalassa*'s RD Instruments 75 kHz Ship Acoustic Doppler Current Profiler, referred to as the SADC in the following. The four beams of the instrument pinged every 2 or 3 seconds, and velocity profiles were calculated as ensemble averages of 20 val-

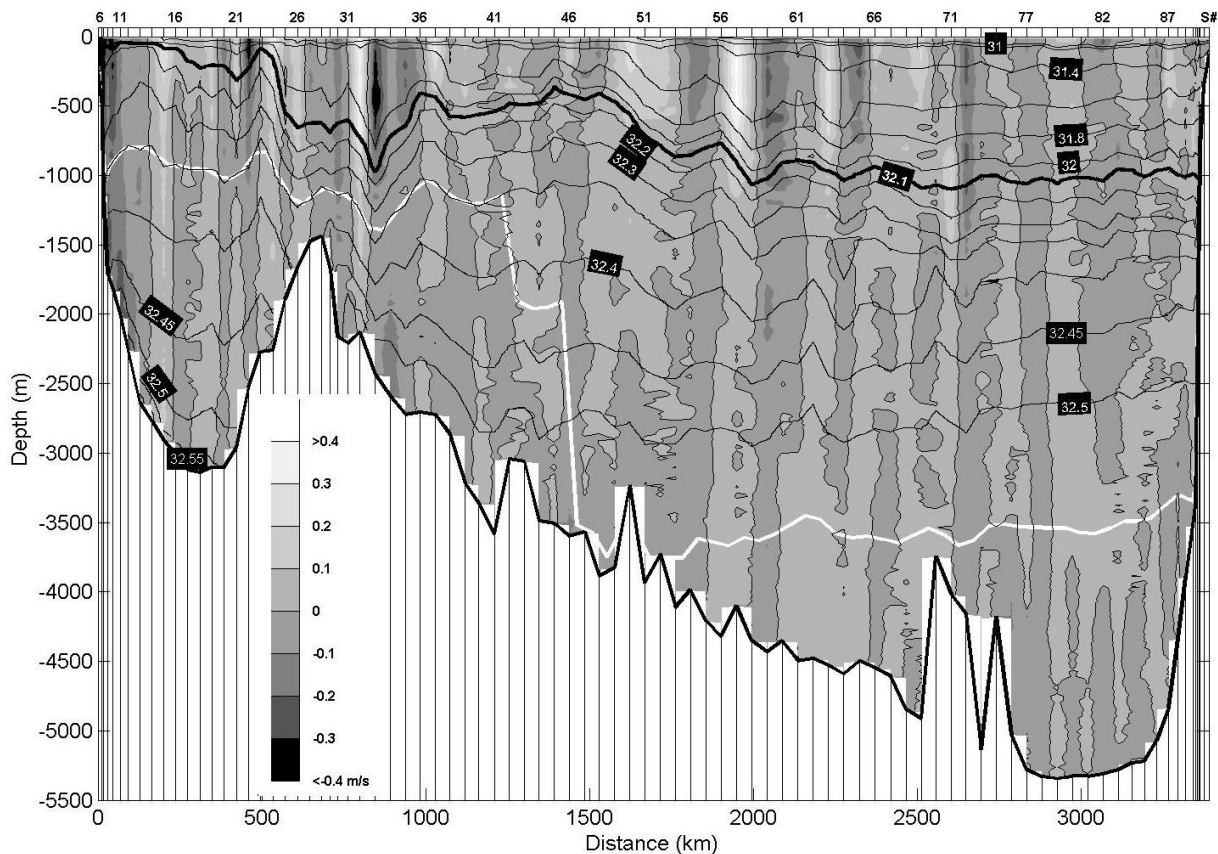


Figure 4. LADCP velocities measured on Ovide 2002 section. Velocities are counted positive northward, and zero contours are underlined. Thin black lines: labelled contours of σ_1 density. Thick white line: reference levels chosen for computing geostrophic velocities.

ues, after removing the ship velocities. A high level of quality was obtained by using combined navigation data from a differential GPS and two gyrocompasses, and by carefully flagging the data using median filters and tests on the vertical velocity and the velocity error estimate. By comparing currents during the stations and underway, we could crudely verify that the ship velocity was correctly removed. The correlation between the ship velocity and the current component along the trajectory during acceleration phases was then minimized by correcting the ADCP alignment by 0.45 degrees. The correction on measured current velocities is small (less than 0.02 m s^{-1}), but since the ship is always moving in the same direction, the cumulative error without the correction would lead to a 30 Sv transport southeastward. Note however that the data tended to get noisier after station 74, which is most probably a consequence of the oligotrophy of the Iberian Basin water. A section of the East Greenland Current (EGC) is shown on Figure 3. The estimated errors on the 20-ensemble mean velocity are of the order of 0.03 m s^{-1} , showing that the measured vertical velocity is mainly noise.

2.3. LADCP Data

The rosette was equipped with a 150 kHz downward-looking and a 300 kHz upward-looking RD Instrument lowered Acoustic Doppler Current Profiler (LADCP). Both LADCPs returned data at every station. Using the inverse method developed by Visbeck [2002], the two data sets were combined to estimate the horizontal velocity profiles at station locations. For 18 stations, data from the 300 kHz upward-looking LADCP were omitted because of their poor quality [Lherminier et al., 2003]. On complex bathymetry features, the influence of the bottom tracking was reduced for 14 stations to the last 50m instead of 300m, thus reducing the effect of lateral reflections. Profiles were then studied one by one and compared with the SADCP station-averaged profiles. For 27 stations where comparison was not satisfactory, LADCP profile calculation took into account SADCP data to improve the first 600 meters.

The section of LADCP currents perpendicular to the Ovide line is plotted on Figure 4. The horizontal gradients of density (see σ_1 isolines on the figure) are consistent with direct measurements of velocities. The SubArctic Front is noticeable at 1700 km (station 51, 51°N), where the main branch of the North Atlantic Current is measured by the LADCP down to 2500m depth. The LADCP measurements underline

the strongly barotropic character of the currents in the Subpolar Gyre, contrasting with the more baroclinic structures in the southern part of the section.

For both SADCP and LADCP, the velocity due to the barotropic tide is estimated using the global 1/4 degree tide model of *Egbert et al.* [1994]. Although the resolution is not suitable on the shelves, we observe that tide currents explain most of the bottom currents on the Iberian shelf, as expected. This is not so clear on the Greenland shelf, as it will be discussed in section 4.2, but we prefer to simply keep the correction as is. All the discussions below use de-tided current data, explicitly noted otherwise.

2.4. ADCP Velocity Profiles

Comparison of on-station SADCP and LADCP velocity profiles is useful to check the quality of the data. Then the averaged profiles between stations are compared to geostrophy and differences are interpreted, as explained hereafter on three examples. Note that for a pair of stations, the SADCP mean profile can be either (i) the average of on-station data, which is then directly comparable to the LADCP mean profile, or (ii) the average of the between-station data. We will show that the latter method is naturally more comparable to geostrophy.

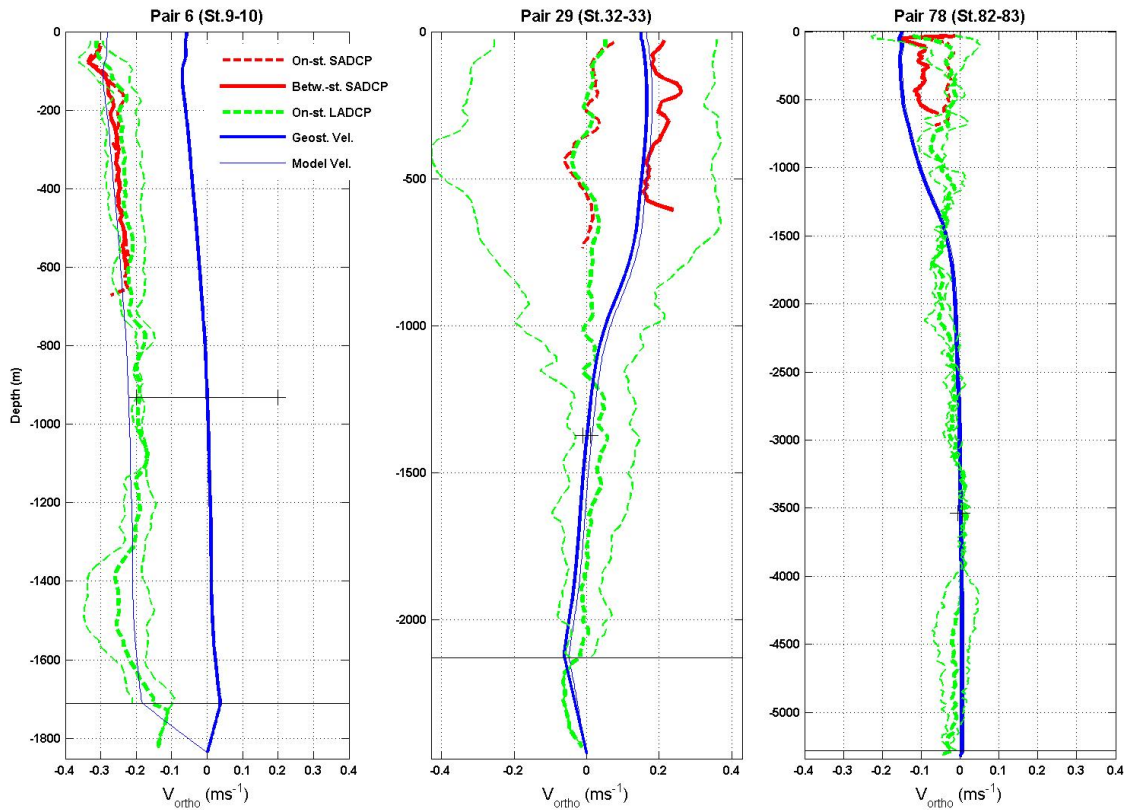


Figure 5. Profiles of the velocity perpendicular to the section at 3 pairs of stations. The red lines are the velocities measured by the SADCP: the average along the route between the stations is the thick line and the average of the velocities at both stations is the dashed line. In green dashed lines are the velocities measured by the LADCP on the rosette: both stations are represented by the thin lines, and the average by the thick line. The blue lines are the geostrophic profiles: a priori (thick) and after inversion (*S-sadcp*, thin). The horizontal thin line delimited by 2 crosses shows the $0 \pm \sigma^i$ range at the reference level for geostrophy. The other horizontal black line indicates the deeper common depth of the pair of stations.

When the circulation is barotropic, the direct velocity measurements differ significantly from the geostrophic profiles computed assuming a level of no motion. This

statement is illustrated by pair 6 (Figure 5) in the East Greenland Current, where all ADCP average profiles show a good agreement, but are shifted from the geostrophic profile although the shear is similar between 100 and 1000m.

Profiles averaged along the route (dashed on Figure 5) can be very different from those averaged on the stations. This is mainly explained by the station spacing of 47 km (reduced to 23 km on steep topography features, and 37 km in the Irminger Sea): any mesoscale feature less than 100 km wide can be mis-sampled. It can be seen on the Eastern side of the Reykjanes Ridge (RR) with the LADCP profiles of stations 32 and 33 (pair 29 on Figure 5): the ship crosses a 1000m-deep eddy that has a diameter of 100 km and velocities of about 0.4 m s^{-1} , but the structure is not symmetrically sampled, so the SADCP average along the route differs by 0.2 m s^{-1} from the station averages (from SADCP and LADCP). In this situation, the average along the route is more consistent with the shear of the geostrophic profile. Note that for this pair, SADCP data were not used to improve LADCP profiles in the surface layer, and the agreement is nevertheless very good.

In the Iberian Abyssal Plain, LADCP velocity profiles were used to confirm the chosen reference level for the geostrophic calculation, as illustrated by the crosses on pair 78 of Figure 5.

3. Estimating The Absolute Velocities with the Inverse Model

3.1. Ekman Transports

The Ekman transports across the Ovide line are calculated from the wind stress of the European Centre Medium range Weather Forecast reanalysis ERA40 [Up-pala *et al.*, 2005]. The value of $-0.95 \pm 0.51 \text{ Sv}$ was obtained by averaging June and July 2002.

3.2. The Box Inverse Model

The absolute geostrophic velocity field perpendicular to the Ovide section was estimated using the following steps. First, geostrophic velocities referenced to selected levels were computed for each station pair. Then, the unknown velocities at the reference levels were estimated by minimizing the weighted sum of:

1. The squared reference level velocities,
2. The squared residuals of transport constraints derived from the SADCP and LADCP measurements,
3. The squared residual of an overall mass conservation constraint.

Noting u_r^i the unknown reference level velocity at station pair i , $T_{adcp}^{i,k}$ the SADCP or LADCP derived transports at station pair i for a depth interval denoted as k , $T^{i,k}$ the corresponding model transports, R the residual of the mass constraint, then the u_r^i minimizes:

$$\sum_{i=1}^{npair} \left(\frac{u_r^i}{\sigma^i} \right)^2 + \sum_{i=1}^{npair} \left(\frac{T^{i,k}(u_r) - T_{adcp}^{i,k}}{\sigma_{adcp}^{i,k}} \right)^2 + \left(\frac{R(u_r)}{\sigma_R} \right)^2$$

where σ^i is the expected amplitude of the velocity at the reference level at station pair i , $\sigma_{adcp}^{i,k}$ the uncertainty on the estimate of the ADCP-derived transport at station pair i for the depth interval k , and σ_R is the error on the mass conservation constraint. $npair$ is the number of station pairs along the Ovide line.

This method is often referred to as "generalized least square inverse". It allows the computation of errors on reference level velocities [Mercier, 1986] and transports [Lux *et al.*, 2000]. Errors on mass and heat transports only include final uncertainties on the reference level velocities. The uncertainties (σ) implemented in the model are discussed hereafter. Transports crossing the section northeastward are counted positive.

3.3. Reference Levels

The reference levels (Figure 4) were first chosen to produce reasonable deep circulation schemes before inversion. In the Irminger Sea and over the eastern flank of the Reykjanes Ridge, the reference levels were set at $\sigma_1 = 32.35$ or at the bottom if shallower. Such a reference level, close to 1000m, produces a deep cyclonic circulation in the Irminger Sea, in agreement with Bacon [1998a]. This choice is close to the minimum current intensity observed in the LADCP data between the East Greenland Current above and the Deep Western Boundary Current (DWBC) below. In the West European Basin and the Iberian Abyssal Plain, the reference level was chosen at $\sigma_4 = 45.84$ or at the bottom if shallower following McCartney [1992]. It gives a net northward geostrophic flow of Antarctic Bottom Water (AABW) of 1.3 Sv, which is a typical value for this water mass transport [McCartney, 1992; Saunders, 1987]. From stations 42 to 46, the reference levels were chosen at $\sigma_2 = 36.94$, consistent with LADCP measurements.

As explained above, the assumption of no motion at the reference level is weighted by the standard deviation σ^i which takes into account the direct current observations. It is chosen wider on the western boundary and around Reykjanes Ridge, where currents are more barotropic (Figure 6).

3.4. Overall Mass Constraint

The mass constraint requires that the sum of the geostrophic and Ekman transports perpendicular to the Ovide line be equal to 1 Sv northward. This value is consistent with the algebraic sum from the $0.8 \pm 0.1 \text{ Sv}$ inflow through Bering Strait [Woodgate and Aagaard, 2005], the $2.6 \pm 1 \text{ Sv}$ export through Davis Strait [Cuny *et al.*, 2005], and the 0.2 Sv estimate for P-E+R in the Arctic [Serreze *et al.*, 2006]. This constraint is also supported by model estimates of the transport from the Subpolar Seas into the Arctic Ocean [Maslowski *et al.*, 2004].

A net error of $\sigma_R = 3 \text{ Sv}$ is applied to the mass balance, following the analysis of Ganachaud [2003], where it is shown that the ageostrophic variability of the ocean

is predominant over the non-synopticity of the measurements in this error estimate.

As a matter of fact, imposing 0, 1 or 1.5 Sv northward for the overall mass balance has no significant impact on the result, as expected from the associated 3 Sv error.

3.5. SADCP constraints

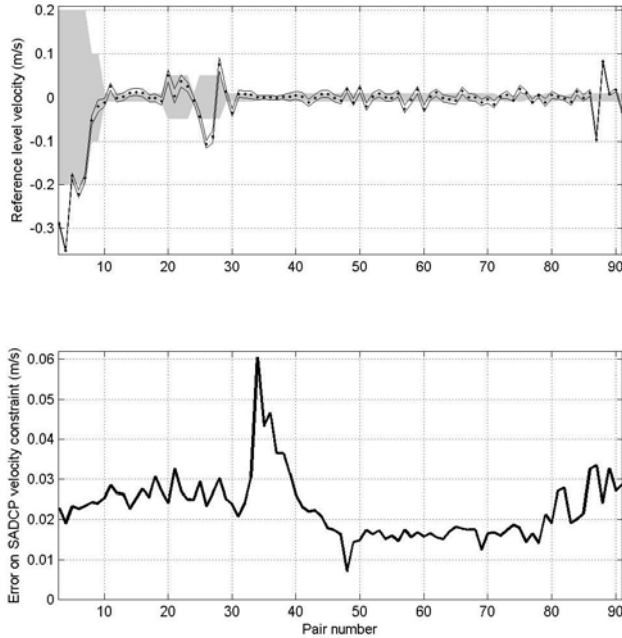


Figure 6. Top: for each pair of station numbered from 3 to 91, velocities at the reference level with errors from the inverse model solution S_{sadc} , on top of σ^i , the expected amplitude as set in the model (grey area). Bottom: calculated errors on SADCP mean velocity between 86m and 310m (or bottom). These values are transformed into transport errors $\sigma_{adcp}^{i,k}$ and implemented directly into the inverse model.

Considering the sampling issues raised in section 2.4, it has been decided to mainly use the SADCP averaged along the ship route to constrain the model. Mass transports can be calculated between 86m and 310m (or bottom) depth for the 89 pairs of stations, by multiplying the measured mean velocity by the distance between stations times the layer thickness. This layer was chosen far enough from the surface to neglect the Ekman contribution, and above the depth where the signal to noise ratio weakens.

Estimating the transport estimate uncertainties $\sigma_{adcp}^{i,k}$ is important for the following study, since it conditions the influence of the SADCP data on the final results. The uncertainties has two sources: one is due to the instrumental error, and the other is due to the physical environment, i.e. ageostrophic (mainly inertial-gravity waves) and fine-scale currents, which scaling is assumed to be smaller than a few kilometers. For each pair of

stations, the between-station route is divided into N independent 5-kilometer segments. The velocity standard deviations (std) are calculated between 86m and 310m depths for all the segments, representing the contributions of the two uncertainty sources. The velocity uncertainty is then deduced from the vertical and horizontal averages of the std values divided by \sqrt{N} . Uncertainties are found between 0.01 and 0.06 m s^{-1} for the whole section (Figure 6). They are quite representative of meteorological conditions with rough seas associated with larger error for pairs 34 to 39, and of the decreasing backscatter in the southern part of the section.

For 7 pairs of stations in the Iberian Abyssal Plain, SADCP data were unreliable because scattered occasional gaps led to an inappropriate sampling of the velocities along the route. In these cases, we chose to reduce the tolerance on the velocity at the reference level, thus reinforcing the hypothesis of no motion at this level. The pair 78 on Figure 5 is one of these pairs. For all of them, we could verify that LADCP measured velocities are close to zero at the reference level, as shown by the crosses on the figure.

The inversion referred to as $S\text{-}sadcp$ in the following uses the SADCP transports between 86 m and 310 m depth and mass conservation to constrain the model at all station pairs.

3.6. LADCP constraints

Table 1. LADCP transports and errors by region in Sv. Layer 1 is defined from the surface to $\sigma_2 = 36.95$, and layer 2 from $\sigma_2 = 36.95$ to the bottom. Regions are plotted on Figure 2. "B." states for Boundary, "C." for Current, "O." for Overflow and "W." for Water.

Region	Layer	Stations	Transport
East Greenland C.	Layer 1	5 - 14	-28 ± 4
Deep Western B. C.	Layer 2	5 - 17	-9 ± 3
Irminger Sea	Layer 1	14 - 27	$+19 \pm 11$
Irminger Sea	Layer 2	17 - 27	$+4 \pm 4$
East Reykjanes	Layer 1	27 - 42	-18 ± 14
Iceland Scotland O. W.	Layer 2	27 - 42	-13 ± 3
North Atlantic C.	Layer 1	42 - 62	$+19 \pm 11$
North Atlantic C.	Layer 2	42 - 62	-10 ± 6
North Atlantic C. 2	Layer 1	62 - 75	$+8 \pm 15$
North Atlantic C. 2	Layer 2	62 - 75	$+8 \pm 8$
Iberian Basin	Layer 1	75 - 87	-8 ± 8
Antarctic Bottom W.	Layer 2	75 - 87	-3 ± 10
Eastern B. C.	Layer 1	87 - 96	$+5 \pm 2$
Eastern B. C.	Layer 2	87 - 96	-1 ± 3

Using LADCP velocity profiles to add information to the model is not straightforward when one considers the sampling issue explained in section 2.4. There are also other sources of local noise, due to a lack of scatterers in the water and to the influence of ageostrophic currents. While weak backscattering levels are more noticeable at depths below 2000m, the first 1000 meters are af-

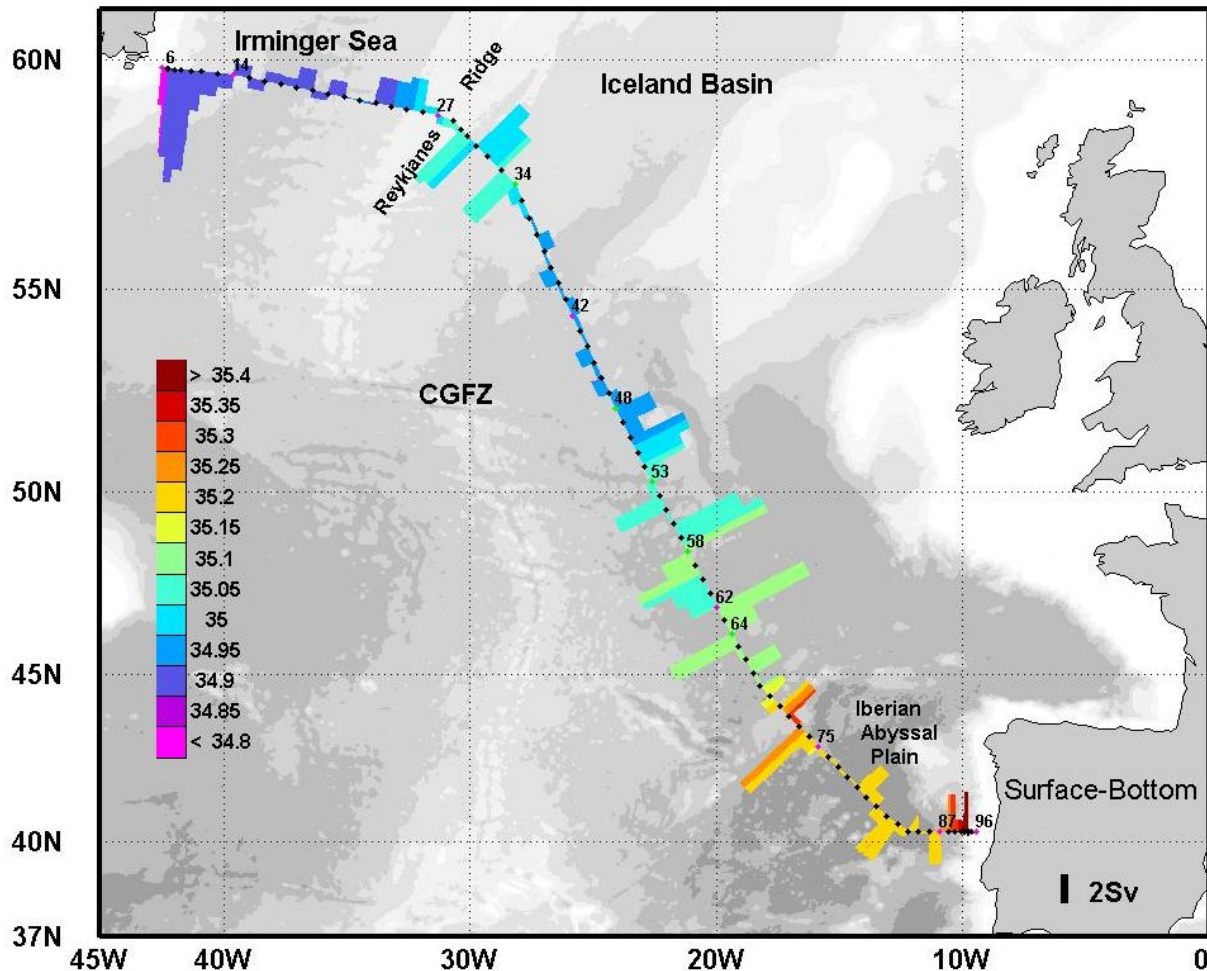


Figure 7. Vertically cumulative transports calculated from the S-sadcp run and plotted on the North Atlantic bathymetry, overlaid with the mean salinity of the water column at the corresponding location (in color). The dots are the stations.

ected by small scale baroclinic currents, as could be observed by comparing geostrophic vertical shear with LADCP measurements. For instance, internal tides can be seen on steep topographic features. So constraining the model with individual profiles introduces inconsistencies with the geostrophic transport estimates.

Instead of constraining the model by individual station pair data, a more satisfying solution is found by calculating LADCP integral transports for 7 regions and 2 layers (separated by $\sigma_2=36.95$). Table 1 gives the corresponding transport values used in the inverse model. The regions have been carefully chosen to describe the main current systems, and, therefore, add useful information to the geostrophic estimates. The transport errors $\sigma_{adcp}^{i,k}$ are estimated by incorporating a sampling error calculated as the rms of the transport differences between the 2 stations of the pairs. Based on the overall mass balance of the LADCP section, a 0.001 m s^{-1} bias error is included in the error estimates listed in Table 1.

The inversion referred to as *S-ladcp* hereafter uses the LADCP transports of Table 1.

3.7. Summary of model setup

The solution of the model that only takes into account the overall mass constraint of $1 \pm 3 \text{ Sv}$ is referred to as *S-geost*. In the solutions *S-sadcp* and *S-ladcp*, the current measurements were added as constraints for each pair of stations in S-sadcp, or for 7 regions and 2 layers in S-ladcp. In all the following discussion on transports, the *S-sadcp* solution is used, explicitly stated otherwise.

4. Transports

4.1. The Vertically Cumulative Transport

The vertically cumulative transports of S-sadcp are discussed hereafter (Figure 7). The salinity allows us to identify the water masses that dominate in the water column.

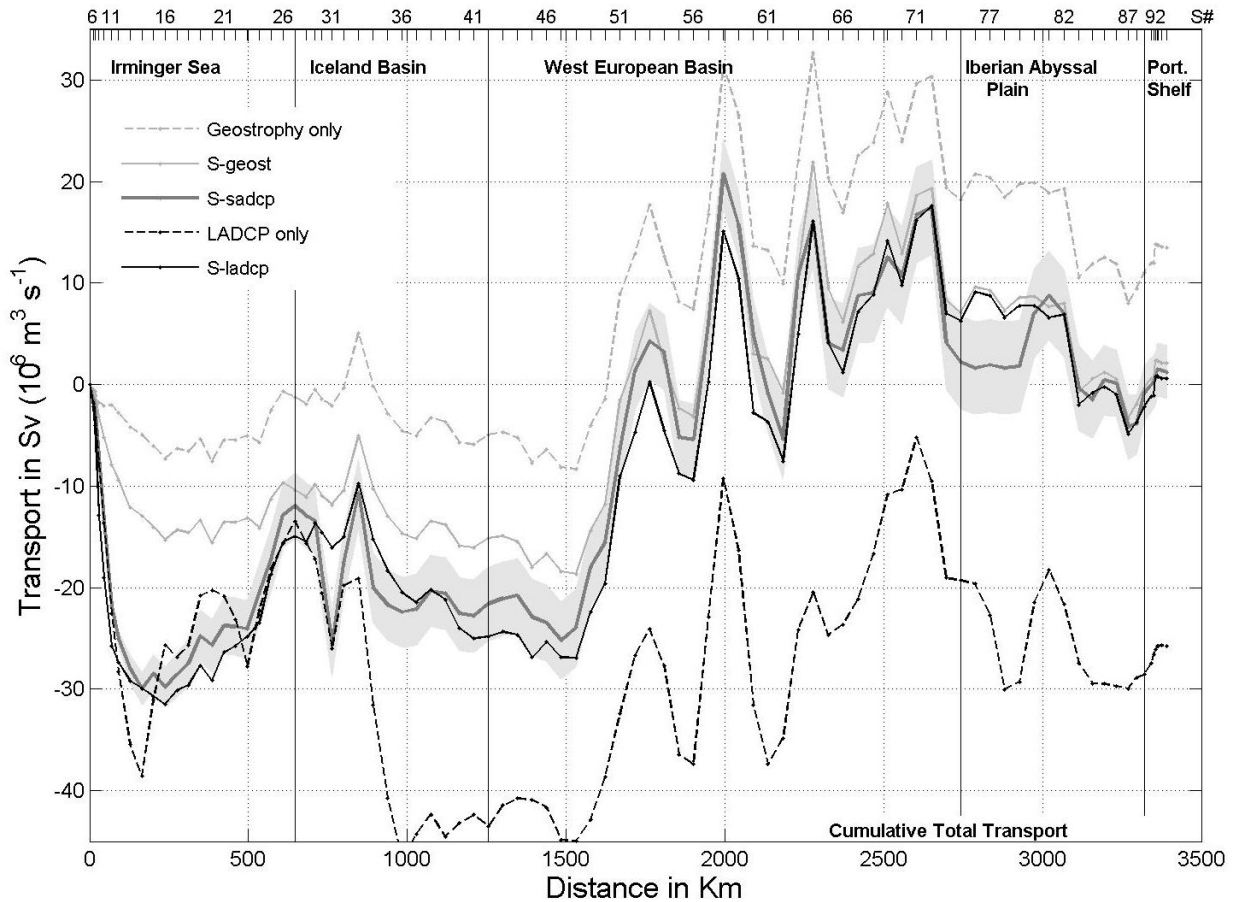


Figure 8. Vertically integrated cumulative transport from Greenland (left) to Portugal (right), plotted against distance along the Ovide section, with station numbers labelled at the top of the plot. Positive values indicate northward transport. The geostrophic (dashed grey) and LADCP (dashed black) transports are from data only. The 3 other lines are from model inversions: light grey with mass conservation as the only constraint (S-geost), thick dark grey with mass conservation and SADCP constraints on each pair (S-sadcp) and black with mass conservation and LADCP constraints by region (S-ladcp). The red shaded region indicates the uncertainty in the S-sadcp solution.

In June 2002, the East Greenland Coastal Current (EGCC), flowing southward, carried ice that prevented any measurement over the shelf but highlighted the role of this current for the fresh water balance of the Arctic [Bacon *et al.*, 2002]. At the northern tip of the section, the low salinity indicates the influence of the EGCC. Between stations 7 and 6, the surface salinity decreases from 33.35 to 32.35, which corresponds to the salinity at the eastern edge of the EGCC in 1997 [Bacon *et al.*, 2002]. Since the 215m deep western station (6) is just inshore of the shelf break, we suppose that the EGCC was not fully sampled in 2002 due to the ice cover, and

according to Wilkinson and Bacon [2005], we expect to miss at most 0.7 Sv flowing southward. This 0.7 Sv is therefore added to the final transport uncertainties in the model solutions.

Away from the shelf, the whole current system in the Irminger Sea is characterized by a mean salinity between 34.88 and 34.92, with a marked cyclonic circulation. On its southeast edge, the aforementioned anticyclonic circulation around the Reykjanes Ridge (RR) between stations 25 and 31 is in the immediate vicinity of a strong anticyclonic mesoscale feature between stations 31 and 34 (see also Figure 2). Travelling toward the South-East, the next noticeable feature is the already mentioned North Atlantic Current beginning at

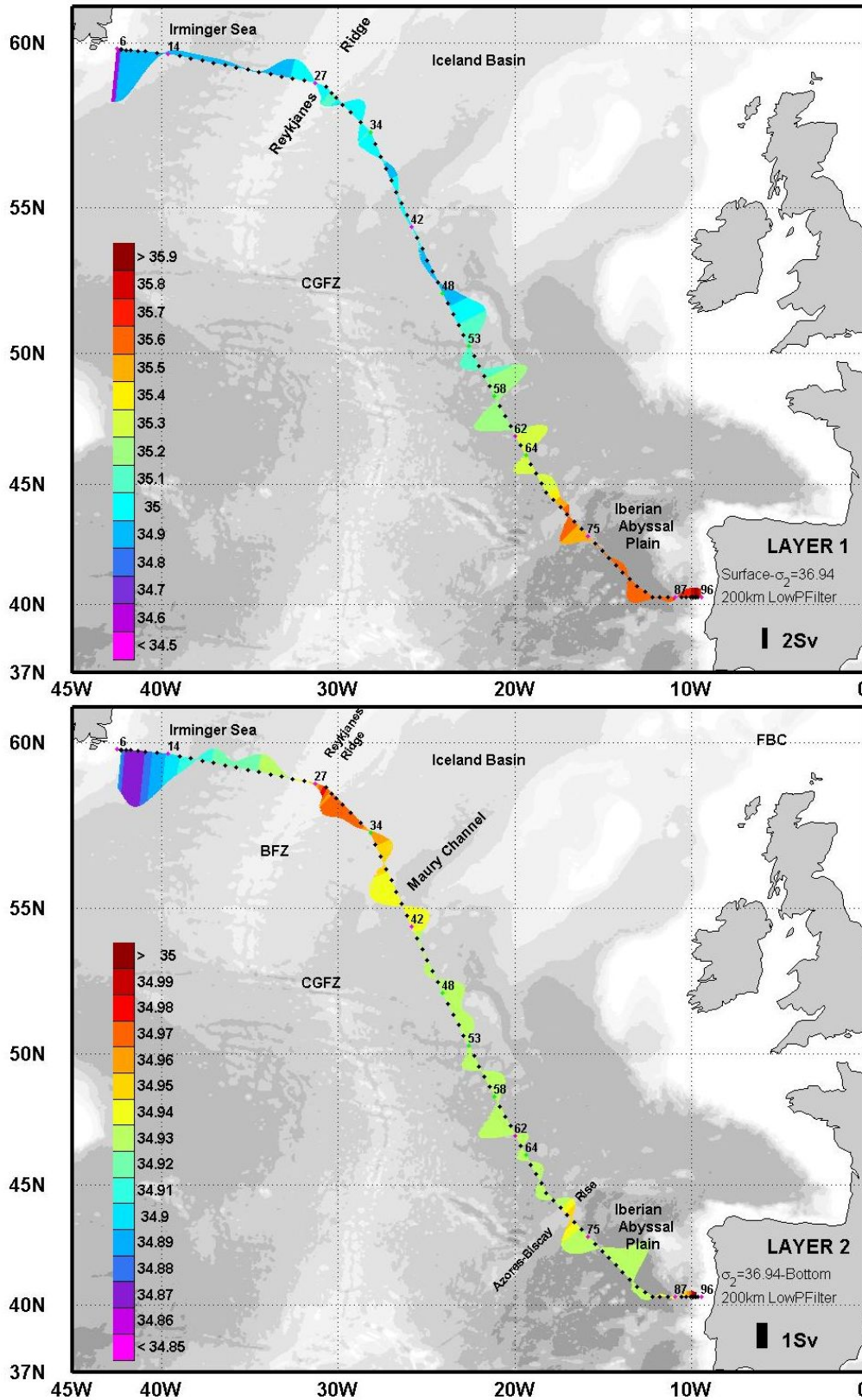


Figure 9. Same as figure 7, but for layers between the surface and $\sigma_2 = 36.94$ (top) and between $\sigma_2 = 36.94$ and bottom (bottom). Transports have been low-pass filtered with a cut-off wavelength of 200 km to enhance large scale patterns.

station 48, and followed by 3 mesoscale patterns cen-

tered on stations 53, 58 and 64, which transports are more easily quantified on Figure 8. The positive salin-

ity anomaly at station 72 centered around 1000m depth (Figure 2) is wrapped by a strong anticyclonic circulation of 8 ± 4 Sv, which is consistent with the description of a 100 km wide meddy, and marks the northern limits of the Iberian Abyssal Plain and of the Mediterranean Water spreading across the Ovide section. The other salinity anomalies are not easily associated with any particular circulation patterns that could lead us to identify them as isolated structures. The last noticeable feature is the 2.1 ± 0.4 Sv Eastern Boundary Current on the Iberian slope and shelf, between stations 89 and 96.

The same circulation patterns can be observed on Figure 8, where transports have been accumulated from Greenland to Portugal. From this figure, we observe a residue of +12 Sv in the geostrophic measurements and -25 Sv in the LADCP cumulative transports. The most significant bias of the latter is caused by stations 32-

33 discussed with Figure 5. However, another similar sampling error occurs in an eddy of the DWBC (stations 15-16) and affects the western current system in the Irminger Sea; this quite barotropic eddy can actually be seen on Figure 3. Note that despite these issues, integrating directly measured current data by region allows us to obtain two similar results for *S-sadcp* and *S-ladcp*. By incorporating the current data, we get a more barotropic Irminger Gyre, the magnitude of which is increased from 8 to 20 ± 4 Sv. The circulation around the RR found in most models [Treguier *et al.*, 2005] and in float data [Lavender *et al.*, 2000] is also greatly enhanced, leading to a total transport of 7-13 Sv centered on station 27 (the top of the ridge). Next to it, the anticyclonic circulation magnitude reaches 10 ± 5 Sv. Southeast of RR, influence of the ADCP data decreases, as would be consistent with a more baroclinic circulation.

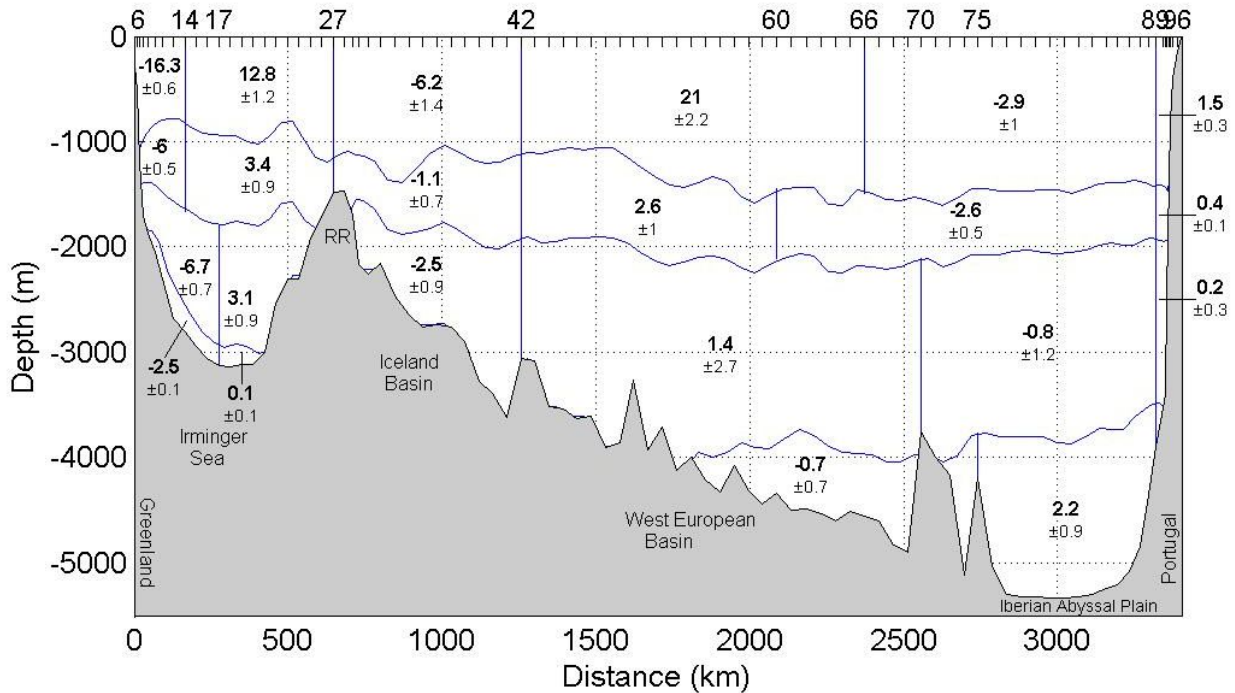


Figure 10. Transports in Sv crossing the Ovide section in 2002 (*S-sadcp* solution), integrated over boxes. The errors are given by the model after inversion. Layer limits are $\sigma_1 = 32.35$, $\sigma_2 = 36.94$ and $\sigma_4 = 45.85$.

The transports for the upper and lower layers are presented on Figure 9. The limit between the layers is fixed at $\sigma_2 = 36.94$; this isopycnal is very similar to the usual $\sigma_0 = 27.8$ limit in the northern half of the section,

and it has the advantage of not varying rapidly along track in the southern half, where it lies around 2000 meter depth. Note that it is also located in the core of the Labrador Sea Water, as indicated by the relative minimum of salinity and maximum of oxygen on Figure 2c. To better localize large scale features on Figure 9, the

transports were filtered with a 200 km low-pass filter along the section. In order to analyse the transports by region, the upper and lower layers are subdivided in two layers on Figure 10. The four resulting layers are delimited by $\sigma_1 = 32.35$ (above the LSW and sim-

ilar to $\sigma_2 = 36.874$ of Bacon [1997]), $\sigma_2 = 36.94$ and $\sigma_4 = 45.95$ (above the Antarctic Bottom Water). All these figures will be used to describe the main circulation patterns in June 2002.

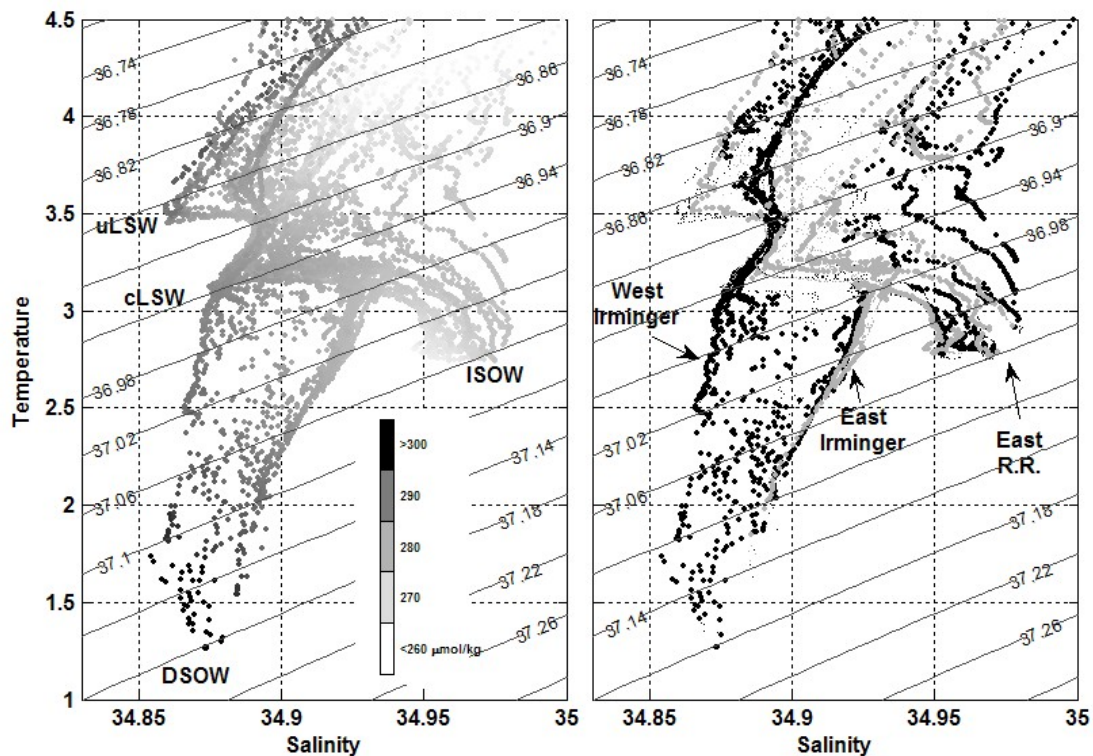


Figure 11. θ - S diagrams of station 6 to 42. Properties have been averaged in 10 meter layers for each pair of stations. On the left diagram, each point is colored according to its oxygen value. On the right diagram, black (grey) points figure southwestward (northeastward) velocities in the model, respectively, and large dots indicate velocities greater than 0.1 m s^{-1} .

4.2. Upper Layer Circulation ($\sigma_2 < 36.94$)

It is believed that barely 2 Sv of the East Greenland Current (EGC) comes from the Nordic Seas fresh boundary current, and a major part of this current at 60°N derives from the Irminger Current circulating from the RR and entraining Irminger Sea water on its way [Pickart *et al.*, 2005]. That is why, at this latitude, the EGC is also called the East Greenland/Irminger Current (we will keep EGC for simplicity in the following). Property sections definitely show strong salinity gradients within the current that both drive the

geostrophic flux and testify to the dual origin of the EGC. This strong current is relatively narrow (165 km width, between stations 6 and 14) and extends from the shelf break and the 2800m isobath. When calculated above the $\sigma_2 = 36.94$ isopycnal, its transport is estimated at 22 Sv southward (Table 2). Bacon [1997] estimated 21 Sv for the EGC transport at 60°N (from the surface down to $\sigma_2 = 36.944$). This value is surprisingly similar considering the known variability of the East Greenland Current at short time scale, but models also show that this variability is minimum in summer, consistent with a weaker wind forcing [Treguier *et al.*, 2006]. Furthermore, Bacon [1997] also uses ADCP data

and an inverse model to obtain this value, and the overall mass transport constraint used in both models tends to damp the variability at very short time scale (a few days).

Table 2. 2002 transports in the main currents of the North Atlantic (positive northward). Errors are estimated by the inverse model. The East Greenland Current (EGC) is defined here with $\sigma_2 < 36.94$ (equivalent to $\sigma_0 < 27.8$). DWBC stands for Deep Western Boundary Current (off Greenland), DBC for Deep Boundary Current, RR-E and RR-W for the Reykjanes Ridge East and West, DSOW for Denmark Strait Overflow Water. All the deep transports (DWBC, DSOW, DBC) are calculated using $\sigma_2 > 36.94$. The North Atlantic Current (NAC) is defined with $\sigma_1 < 32.35$.

Region	Ovide sta.	Transport (Sv)
EGC	06-14	-22.4±1.1
DWBC	06-17	-9.2±0.9
DSOW	06-17	-6.0±1.3
RR-E DBC	17-27	+3.2±1.0
RR-W DBC	27-42	-2.5±0.9
NAC (net)	42-96	+19.6±1.7

The cyclonic Irminger gyre is well defined in the circulation schemes derived from surface drifters [Fratantoni, 2001; Reverdin et al., 2003; Flatau et al., 2003]. During Ovide, the signature of this cyclonic circulation was a doming of the isotherms and isopycnals between stations 5 and 26 (Figure 2a), a feature that might favour local convection during severe winters [Bacon et al., 2003; Pickart et al., 2003]. On the same figure, the oxygen section shows a relative maximum down to 800m depth at station 12, as do CFC data discussed in Forner [2005], at the off-shore edge of the EGC. It could possibly be related to locally convected water but has θ -S characteristics of upper Labrador Sea Water (uLSW, see Figure 11). Another O_2 maximum characteristic of the classical Labrador Sea Water (cLSW) lies at about 1500m. Upper LSW is also seen in an anticyclonic eddy at station 20, embedded in saltier and less oxygenated water influenced by the North Atlantic Central Water (NACW).

A question is to determine how the Irminger cyclonic circulation is embedded into a larger circulation scheme. Connections between the Irminger gyre and the NAC over the Reykjanes Ridge (RR) were suggested by surface drifters [Krauss, 1995; Flatau et al., 2003] and at intermediate depth by floats [Lavender et al., 2000]. On the Ovide section, the θ -S- O_2 properties in the east Irminger Sea show a strong mesoscale variability and a significant interleaving. The connexion with the NAC is observed, but not straight through the RR. Indeed, the Sub-Arctic front, that delimits the eastern Subpolar Gyre at stations 48-53, is also intersected twice in the vicinity of the RR: at stations 23-25 and stations 35-37 (Figure 2). The absolute dynamic topography measured by satellite altimetry (Figure 12) consistently

suggest an anticyclonic surface circulation around RR. This anticyclonic circulation encompasses a pool of sub-polar mode water that is identified around station 33 by its homogeneity and its salinity greater than 35 (Figure 2). The larger thickness of the mode water is within the already mentioned anticyclonic eddy centered at station 33. The eddy core, found at 500m depth (Figure 4), has no clear surface expression (Figure 12).

The main branch of the North Atlantic Current is found at 52°N (stations 48-51, Figures 8 and 9a), 50 km south of the latitude of the Charlie Gibbs Fracture Zone (CGFZ), which marks the northern most limit of this NAC branch [Sy, 1988; Belkin and Levitus, 1996; Schott et al., 1999]. A second branch, less intense, is observed at stations 62-63. Eddies are embedded between these two branches (Figure 9a et 12). We estimate 21 ± 2 Sv for the transport of the NAC between 52°N and 45°30'N (Figure 10, first layer between stations 42 and 66), a value that is weaker than some estimates (about 35 Sv between 40°N and 54°N in Cunningham [2000] and Paillet and Mercier [1997]) but consistent with the 19 Sv at 52°N in Bacon [1997].

South of the 44°N meddy already mentioned in the previous section (station 71), a southward net transport can be identified on Figure 10. This southward circulation in the Iberian basin has been documented by Paillet and Mercier [1997], and amounts to 3 ± 1 Sv in the NAC layer ($\sigma_1 < 32.35$) in 2002. It is of particular importance for the southward advection and subduction of the eastern North Atlantic Mode Water formed in the deep winter mixed-layer to the north of the Ovide section.

A net warm water transport of 19 Sv across a zonal section at 52°N was found in 1991 by Bacon [1997], and it can be compared to the net 19.6 Sv crossing the Ovide section in June 2002 east of 27°W (stations 42 to 96, Table 2).

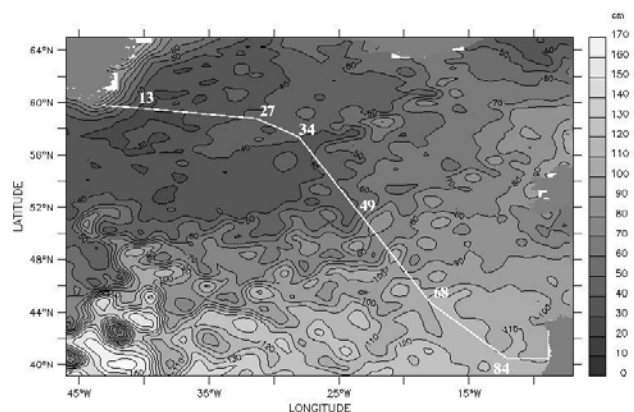


Figure 12. Merged Absolute Dynamic Topography in cm calculated for June 26, 2002 (from the AVISO Live Access Server). The Ovide track is superimposed in white.

4.3. Lower Layer Circulation ($\sigma_2 < 36.94$)

The Iceland-Scotland and Denmark Strait overflows are the two sources of the North Atlantic Deep Water coming from the Nordic Seas. The Ovide line intersected the DWBC transporting the Iceland-Scotland Overflow Water (ISOW) on the eastern side of the RR upstream of the Charlie Gibbs Fracture Zone (CGFZ). This branch transports 2.5 Sv southward (Figure 10, Table 2), similar to the mean transport value reported by *Saunders* [1994] in the CGFZ for $\sigma_0 > 27.8$. From Figure 9b, two peaks of southward flow can be observed: one on the slope of RR, associated with a maximum of temperature and salinity (Figure 2), and a deeper one, partly associated with a deep cyclonic circulation in Maury Channel [*Harvey and Theodorou*, 1986]. The properties of both branches can be seen on Figure 11: they constitute the saltier deep water of the θ -S diagram, lying from $S=34.95$, $\theta=2.76^\circ\text{C}$ for the deeper (eastern) branch to $S=34.975$, $\theta=3.25^\circ\text{C}$ for the slope branch, richer in oxygen. In the deeper branch, we also observe a relative maximum in the amount of silicate (greater than $15 \mu\text{mol kg}^{-1}$: P. Morin, personal comm.). So from the analysis of their hydrological properties and from the deep circulation scheme shown by *Schmitz and McCartney* [1993] (their Figure 12), we conclude that the water of the deep branch transports ISOW from the Faroe-Bank Channel and undergoes the influence of upwelled AABW circulating cyclonically around the north-east Atlantic. This dataset does not bring clues on the origin of the upper branch: according to *Harvey and Theodorou* [1986] or *van Aken and Becker* [1996], it could come from the sills west of Faroe Islands as well as from the Faroe-Bank Channel.

In the eastern half of the Irminger Sea, the deep northward flow found between stations 17 and 27 (Figure 9b) amounts to 3.2 Sv (Figure 10, Table 2). The core of this flow is made of ISOW and classical Labrador Sea Water (cLSW), forming a distinct elbow at $\theta=3.1$ - 3.25°C and $S=34.92$ - 34.93 on Figure 11b, with northward (grey) velocities. The deep cyclonic circulation in the Irminger Sea is revealed by the θ -S characteristics of its eastern limb which is influenced by Denmark Strait Overflow Water (DSOW, Figure 11a). Estimating the amount of recirculating deep water is difficult since the errors on the flows around RR add up to 1 Sv. Furthermore, we found that 80% of the additional 0.7 Sv flowing northward West of RR (as compared to East of RR on Figure 10) lay between $\sigma_2 = 36.94$ and $\sigma_2 = 36.98$, i.e. in the cLSW layer, and we would need a careful tracer analysis to separate the recirculating LSW

from the directly imported one (along the path shown in *Lavender et al.* [2000]).

The DWBC off Greenland transports 9.2 ± 0.9 Sv (Figure 10, Table 2), and it mainly lies between 1700m and 2900m, with an intense barotropic flow inshore of the 2000m isobath, and a more moderate and mainly baroclinic flow offshore. Although the position of the current is consistent with observations in 1987-1990 reported by *Dickson and Brown* [1994], its transport is weaker than the 13 Sv previously estimated at Cape Farewell. One might object that we are dealing with a snapshot in an area of strong variability at a scale of a few days, as underlined by mooring measurements of *Dickson and Brown* [1994]. However, in mooring estimates, part of this variability may be spatial and not temporal, and the integration performed by our geostrophic estimates might smooth out this part. Furthermore, the interannual variability of the DWBC transport was consistently documented by *Bacon* [1998a] from hydrographic sections. For comparison with this latter work, we split our DWBC transport into a baroclinic contribution (5.2 Sv) and a reference level velocity contribution (4 Sv). The baroclinic contribution to the DWBC observed during Ovide is similar to values reported by *Bacon* [1998a] for the late 1990s (4-5 Sv). During the 1980s, the DWBC transport was larger by about 3 Sv.

The relative contribution of DSOW in the 60°N DWBC can be evaluated in Ovide, since no deep sill exists between Iceland and 58°N , where the section crosses the RR: all the ISOW and LSW must cross the section northward west of the ridge (3.2 ± 1.0 Sv Figure 10) before recirculating in the 9.2 Sv DWBC. So we obtain an estimate of 5-7 Sv for the transport of DSOW, which includes entrainment between Denmark Strait and 60°N .

The deep circulation in the West European Basin is mainly influenced by the spreading of the Labrador Sea Water (*Paillet et al.* [1998]). The volume transport integrated between $\sigma_1 = 32.35$ and $\sigma_2 = 36.98$ and accumulated from Greenland to Portugal is shown on Figure 13. According to Figure 2, this plot is representative of LSW transport between the RR (station 28) and 45°N (station 67). About 4 Sv of LSW is found to cross the section northward under the main branch of the NAC, between $51^\circ30'\text{N}$ and $52^\circ30'\text{N}$, while about 2 Sv flows southward above ISOW east of the RR. This implies a net export of 2 ± 1 Sv toward the Iceland Basin, as found in *Bacon* [1997]. In the eastern Irminger Sea, two additional Sverdrups come from the South-West (the Labrador Sea and the Irminger cyclonic gyre), as discussed earlier, while about 4 Sv of uLSW (or Irminger Sea Water) is exported above the DWBC.

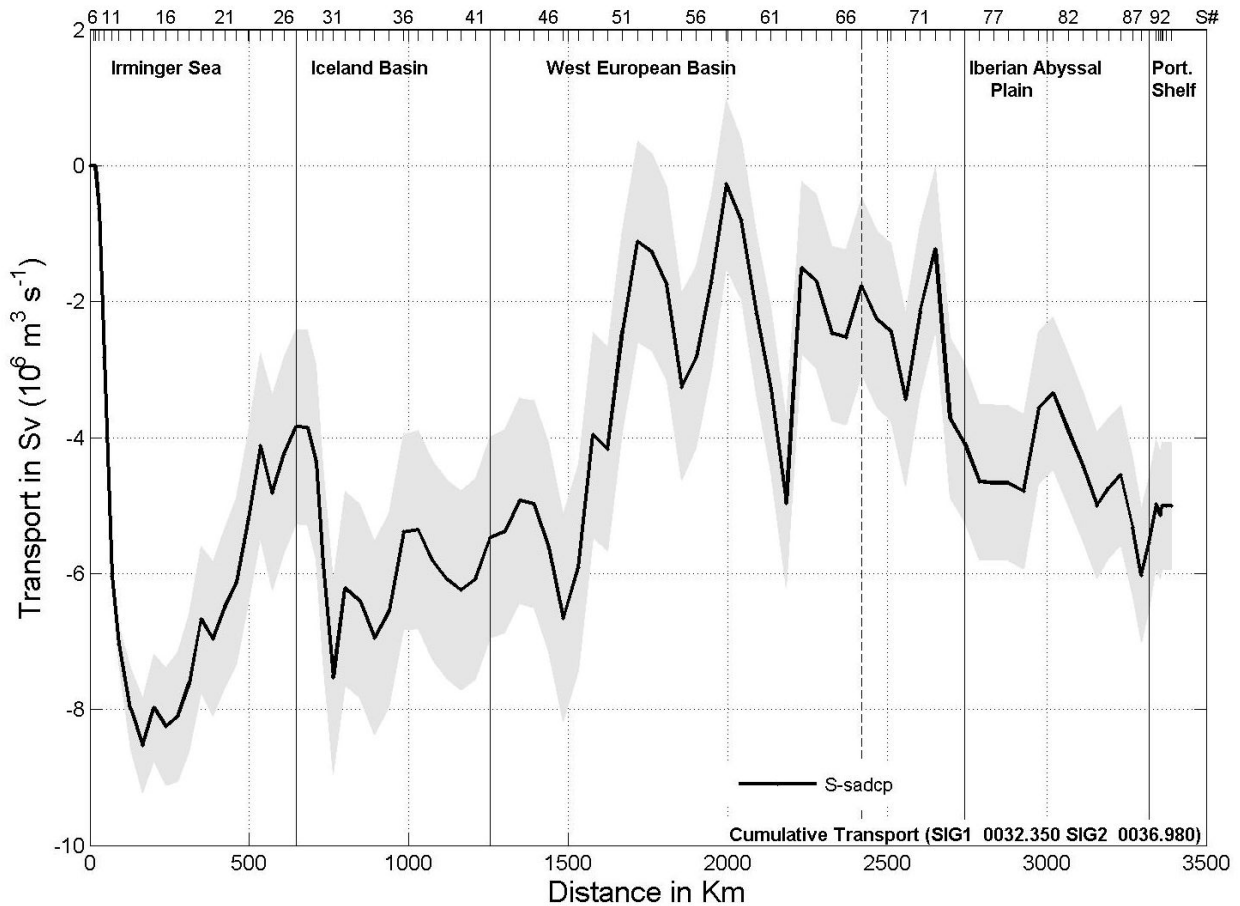


Figure 13. Cumulative transport from Greenland (left) to Portugal (right), vertically integrated between $\sigma_1 = 32.35$ and $\sigma_2 = 36.98$ (see Figure 2), and plotted against distance along the Ovide section (as in Figure 8). Station numbers labelled at the top of the plot.

We know from *Paillet et al.* [1998] that due to its orientation, the section may intersect a meander of the south-eastward spreading of the LSW, with a weak signature in the transports perpendicular to the section. In the data, the south-westward flow that is supposed to underline the southern limit of the LSW influence is not clearly observed due to the predominance of the mesoscale circulation.

In the Iberian Abyssal Plain, a net northward flow transports 2.2 Sv of Antarctic Bottom Water and Lower Deep Water (Figure 9b, stations 75 to 89). One third of this deep flow recirculates cyclonically north of the Azores Biscay Rise (stations 54 to 70), while two thirds are upwelled and flows northward with the Lower Deep Water.

5. Fourex 1997 Revisited with ADCP Data

5.1. Presentation of the Fourex Reanalysis with ADCP Data

The Fourex section (Figure 1) has already been analysed and interpreted in terms of physical and biogeochemical transports by *Álvarez et al.* [2004] (hereafter referenced to as A04). Current measurements from 150kHz SADCPC and LADCP were not used and the velocity at the reference levels was deduced from average numbers found in the literature. Now using the direct current measurements [*Bacon*, 1998b], the calculation of the transports can benefit from synoptic current values. So the objective is to apply exactly the method described in section 3, without climatological constraints.

As our inverse model is slightly different from the one used in A04 (described in *Álvarez et al.* [2002]), a

first step was to run the model using the exact constraints described by A04. These constraints consist of a 25 ± 1 Sv total southward flow from Greenland to 110 km offshore (EGC), a 2.4 ± 1 Sv southward deep flow in the CGFZ, no net transport of AABW (± 2 Sv), salt conservation ($\pm 35 \times 10^9$ kg s⁻¹). The resulting transports of both models all lay within the respective errors, and we could then proceed to include ADCP data plus overall mass conservation (± 3 Sv) instead of constraints described above.

As explained earlier, SADCP data are more appropriate than LADCP data for bringing information at each pair of stations. However, they were found much too noisy in the south-east part of the section, and unfortunately, LADCP data are also lacking in the same area. Knowing that in this part of the section, transports can be reasonably deduced from geostrophy provided that the reference level is properly chosen, we used SADCP data on 48 pairs of stations (2000 km), from Greenland to station 46 at 45°47'N 24°39'W. Reference levels were chosen as in A04, apart from the following pairs: in CGFZ, the reference level for pairs 62-63 and 64-65 was raised to 3000m and 2500m respectively, to match the shallower level of the topography between the stations, and consistent with the LADCP-measured level of no motion.

SADCP data were given with no variance for each averaged profile on 600m route segments. Relying on Ovide statistical analysis on segments of similar length, we apply a 30 cm s⁻¹ standard deviation to the Fourex SADCP velocities, and from there, transport errors between 32 and 200m (or bottom) are calculated as explained in subsection 3.5.

5.2. Results

A comparison between A04 results and the new inversion of Fourex data is shown on Figure 14. Limits in density are those chosen in A04: four layers separated by $\sigma_0 = 27.7$, $\sigma_2 = 36.98$ and $\sigma_4 = 45.85$. Main differences are summarized in Table 3. The North Atlantic Current intensity has not significantly changed: we find that the A04 value of +27.1 Sv is increased to +28.5 Sv, but these values are found within the errors of the inverse model. We see also that the DWBC along the Greenland slope has not significantly changed either. This current includes the DSOW and part of the ISOW that has circulated in the Irminger Basin.

The two main differences are seen in the East Greenland Current and in the deep flow around CGFZ. Direct current measurements all show a much stronger current in the western boundary of the section. The SADCP constraints lead to an EGC that is 11 Sv more intense than in A04. The LADCP confirms this result, with a 37 Sv southward flow on the whole water column (to be compared to the 36.4 Sv summed over the left boxes of Figure 14 and to the 25 Sv imposed in A04). We

conclude that this particular constraint was too low in A04.

Table 3. Comparison of transports between Fourex inversions in the main currents (positive northward), summarized from Figure 14. Errors are estimated by the inverse model.

Region	Layer	Stations	A04(Sv)	ADCP(Sv)
EGC	$\sigma_2 < 36.98$	83 - 93	-19.7±0.8	-30.8±0.7
CGFZ	$\sigma_2 > 36.98$	54 - 72	-6.4±1.4	-2.2±0.7
DWBC	$\sigma_2 > 36.98$	77 - 93	-8.2±0.9	-7.7±0.7
NAC	$\sigma_0 < 27.7$	03 - 65	+27.1±1.9	+28.5±1.3

The 2.2 ± 0.7 Sv south-westward bottom flux in the CGFZ area below $\sigma_2 = 36.98$ is 3 times weaker in the new results, and most of the difference is found within the 5 station pairs of CGFZ itself. The new result is more consistent with direct current measurements, and is also consistent with simultaneous observations of *Schott et al.* [1999]. The flow calculated below the usual $\sigma_2 = 36.94$ ($\sigma_0 = 27.8$) gives only 1.2 Sv westward, but it includes some eastward flowing LSW, which is once again in agreement with *Schott et al.* [1999]. It can theoretically be compared to the annual average of 2.4 ± 0.5 Sv calculated by *Saunders* [1994] below $\sigma_0 = 27.8$. However, this comparison is misleading if one wants to look at the ISOW southward flow. Indeed, records in central Labrador Sea show a maximum of LSW volume and density between 1990 and 1994 [*Yashayaev and Clarke*, 2005, Figure 2], 0.08 kg m⁻³ denser than in the mid 80s. By 1997, this water has spread over CGFZ, replacing part of the ISOW. So the 2.2 Sv southwestward flow measured in CGFZ below $\sigma_2 = 36.98$ is a more appropriate value for ISOW transport.

Schott et al. [1999] suggest also that the deep flow variability in CGFZ may very well be correlated with the NAC position, by modifying the barotropic north-eastward flow in the area. In the Fourex case, this idea is actually supported by the evidence of a strong surface northward flow, that is found above and south-east of CGFZ. However, surface hydrological properties are not typical of the NAC. It is possible also that there is some variability in the proportion of ISOW entering the Irminger Basin north of CGFZ, through the 2000m deep Bight Fracture Zone at 57°N or the 2400m sill at 55°N.

Figure 9 of A04 shows that ISOW is the major water mass found between stations 54 and 72, and these 2.2 Sv will most likely contribute to the DWBC. The 0.6 Sv found west of RR is mainly ISOW circulating in the Irminger Sea. Thus 1.6 Sv may feed the DWBC south of Fourex.

At 60°N, the DWBC is 9.3 ± 1.1 Sv below $\sigma_2 = 36.98$. Calculated below $\sigma_2 = 36.94$, it sums up to 11.3 ± 1.2 Sv southward.

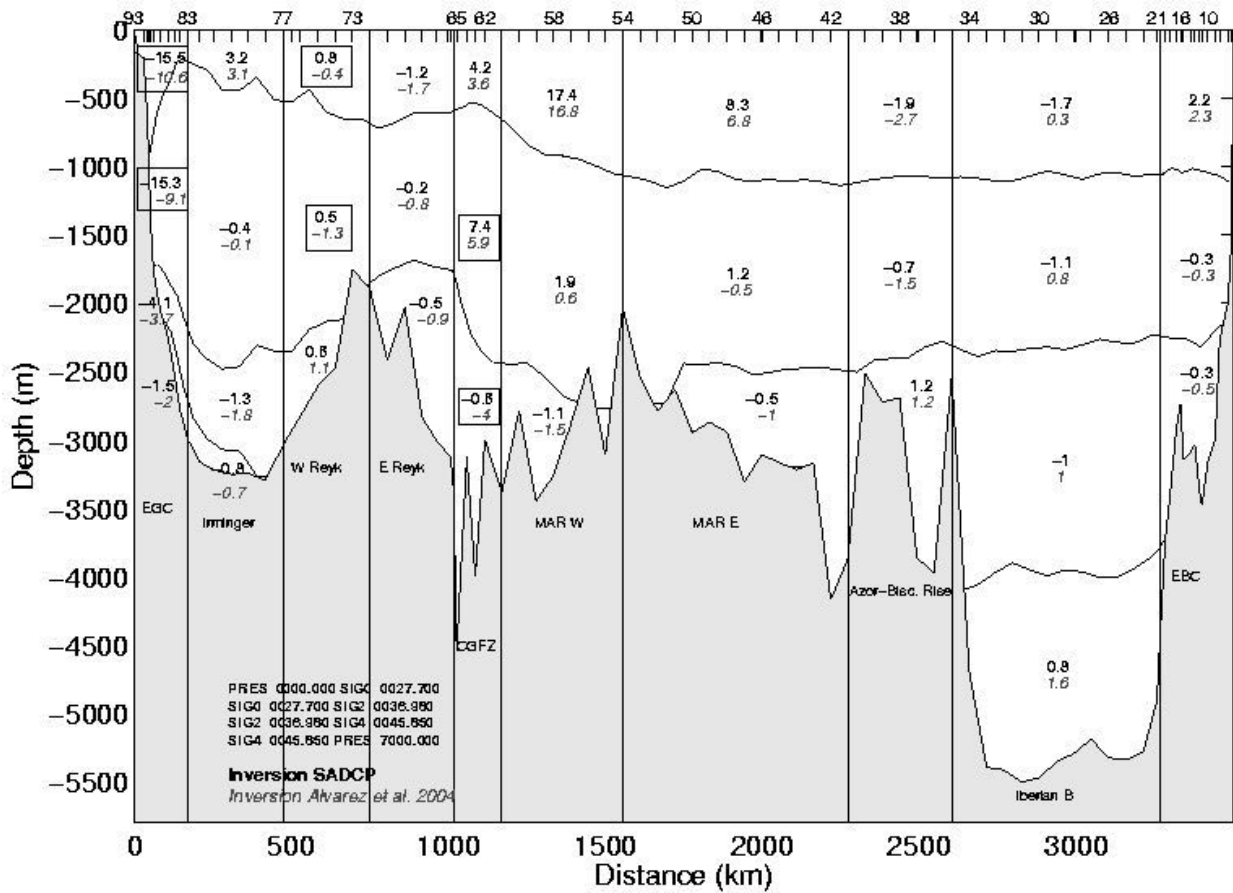


Figure 14. Transports across Foux section (Sv), positive northward. Layer limits are $\sigma_0 = 27.7$, $\sigma_2 = 36.98$ and $\sigma_4 = 45.85$. Faint italic numbers are from Alvarez et al. [2004]. Bold numbers are for the new inversion with SADC data from Greenland to station 46 (at 2000 km). Large differences between both inversions are surrounded with a box.

Finally, it may be noted that the new inversion leads to a slight increase of the northward flow of Labrador Sea Water in the Eastern Basin.

6. Comparison Between 1997 and 2002

6.1. Regional Differences

Ovide 2002 and new Foux 1997 transports can now be compared (Table 2 and Table 4). Because of the different path followed by the two experiments, several difficulties arise in this task.

The DWBC (off Greenland) shows a 2.1 Sv decrease (i.e. about 20%) between August 1997 and June 2002. The relative contribution of LSW, ISOW and DSOW cannot be known in Foux without a careful analysis of the different properties (as done in A04 with the Optimum MultiParameter approach), and this is beyond the scope of this paper. As discussed in section 4.3, it is however possible to separate the contributions of the DSOW and of the other deep waters (ISOW and cLSW) in the Ovide DWBC, as summarized in Table 2.

The NAC can only be compared when calculated globally from the Sub-Arctic Front (SAF) to the Iberian Coast. Although very crude, this estimate takes bet-

ter account of the robustness of inverse models regarding the large scale patterns. For both 1997 and 2002, the subsurface horizontal gradient of temperature has been chosen to localize the SAF. The 30% decrease of the warm water transport northward between 1997 and 2002 is striking and cannot be caused by the different station location. Alarming papers on the subject have already been published [Bryden et al., 2005], but Treguier et al. [2006] show that the NAC variability found along A25 can also be seen in the models, and may very well be due to monthly to interannual variability. This open question may be tackled in a later paper using altimetry data with past and future hydrographic sections (including repeat Ovide surveys).

Table 4. 1997 transports in the main currents of the North Atlantic with the same conventions as Table 2

Region	Foux sta.	Transport (Sv)
EGC	83-93	-27.7±0.6
DWBC	77-93	-11.3±1.2
NAC	03-61	+26.6±1.6

The EGC variability (27.7 Sv in 1997, versus 22.4 in 2002) is also documented by *Treguier et al.* [2006], with a quite surprising match between the CLIPPER model and the data. It is found to be consistent with the weakening intensity of the Subpolar Gyre showed by *Häkkinen and Rhines* [2004].

6.2. Volume Transport as a Function of Depth

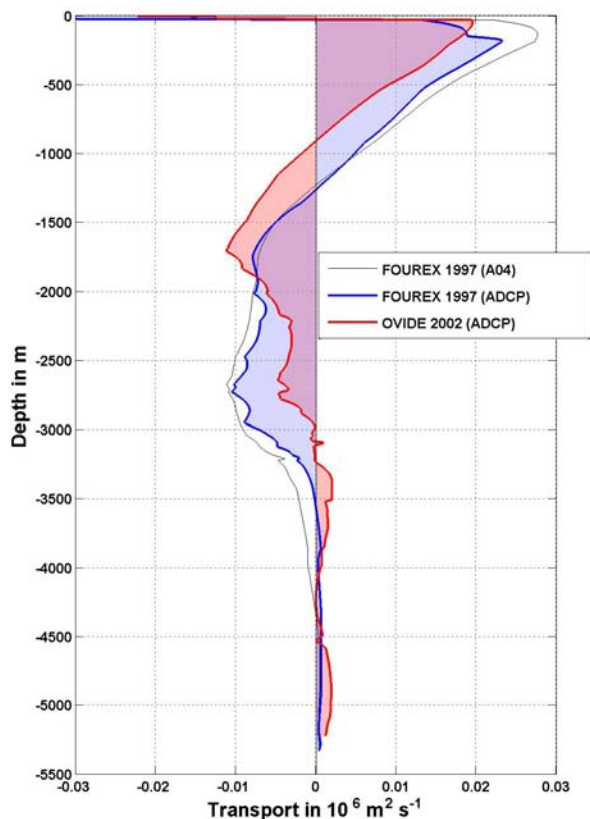


Figure 15. Transport integrated over 1-meter thick layers over the whole section, in $10^6 \text{ m}^2 \text{ s}^{-1}$. The result of Fourex 1997 from *Álvarez et al.* [2004] inversion is the thin black line. The thick black line is from the 1997 ADCP solution, and the thick gray line from the Ovide 2002 ADCP solution. For both lines, the surface of the shaded area underneath gives the net transport in both direction.

The net volume transport associated with the large scale circulation across the section can be calculated in depth coordinates (Figure 15). The MOC strength (MOC_z) is most often calculated as the transport of North Atlantic Deep Water (NADW) [*Marsh et al.*, 2005; *Álvarez et al.*, 2004]. It is represented by the surface of the shaded areas between the two zero crossings at about 1000m and 3500m. The important differ-

ences seen between 1997 and 2002 values (14.2 Sv versus 11.2 Sv, Table 5) come with significant differences in the shape of the horizontally integrated transport on Figure 15.

The northward flow observed above 1300m is mainly the algebraic sum of the NAC and the EGC. In this layer, we observe that the net transport cancels at a much deeper depth in Fourex (1250m) than in Ovide (950m). Inspection of the average depth of the $\sigma_1 = 32.35$ isopycnal and of velocity fields shows that the NAC depth extension is equivalent in Ovide and in Fourex, and cannot explain the different depths of the zero crossing nor the different amplitude of the transport above it on Figure 15. The NAC is 7 Sv stronger in 1997 (Table 4), and is the main factor in the intensification of the northward flow above 1300m, although the net result is moderated by the opposite EGC variability as seen in Tables 2 and 4.

Since we observed that the NAC vertical extension is similar in depth for both years, we conclude that the difference in depth of the zero crossing is mainly driven by the north-eastward transport of LSW which is particularly intense between 1000m and 2000m depth above CGFZ in 1997. Knowing that LSW takes 2 to 6 years to spread over the Mid Atlantic Ridge, the 1990-1994 anomaly mentioned in section 5.2 is likely to create the observed northward transport anomaly above the MAR at LSW depth. This transport is partly compensated in the net balance by the export of uLSW (or Irminger Sea Water, as suggested by A04 following *Pickart et al.* [2003]) at the bottom of the EGC. However, between 1400m and 2500m, this LSW transport anomaly definitely weakens the net south-westward transport on Figure 15.

The southward flow between 1300m and 3000m (3500m in 1997) is mainly formed by the DWBC off Greenland, and is influenced by the currents in CGFZ (in 1997) and along RR (in 2002). It extends deeper in Fourex, mainly because the DWBC is crossed deeper, about 200 km further south, and is more intense in 1997, creating a prevalent feature in the bottom part of the southward transport.

Below 3500m, both inversions show a net northward flow of AABW that forms the eastern branch of the deep cyclonic circulation, the western branch being shallower [*Schmitz and McCartney*, 1993]. The AABW northward flow below 3800m in Fourex transports is weaker than in Ovide (0.8 Sv against 1.5 Sv, Figures 10 and 14), but the associated errors prevent us from interpreting this as a temporal variability.

6.3. Volume Transport as a Function of Density

By Meridional Overturning Cell, we want to refer to the vertical cell composed on the one hand by the North Atlantic Current that feeds the Subpolar Seas with warm water and on the other hand by the Deep Western Boundary Current that brings the Overflow

Waters and the recirculating Labrador Sea Water southward.

We conclude from the previous section that integrating the top or the bottom shaded surfaces of Figure 15 to obtain an estimate (MOC_z) of the MOC is not totally satisfying. Indeed, any slight variation of some horizontal circulation patterns - mainly the EGC, the northward bottom current and the spreading of the LSW - are modifying the value of MOC_z . That is why the transport integrated in layers of 0.1 kg m^{-3} (in σ coordinates) is now examined (Figure 16). Once again, an indication of the circulation strength is given by the surface of the shaded areas. The surface above the zero-crossing corresponds to the maximum cumulative transport northward and defines the Thermo-Haline Circulation (THC) strength according to *Marsh et al.* [2005]. For clarity, we prefer to call it MOC_σ , and we find 19.2 Sv in 1997 as compared to 16.9 Sv in 2002 (Table 5).

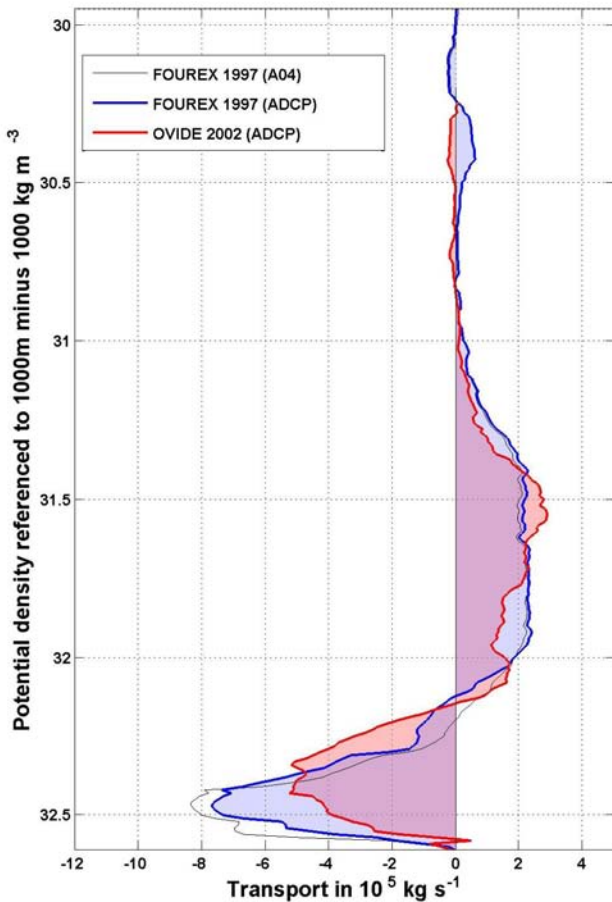


Figure 16. Same as Figure 15, with transport integrated over 0.1 kg m^{-3} density layers over the whole section. Values are in 10^5 kg s^{-1} .

The zero crossing of Figure 16 occurs for $\sigma_1 = 32.1$, both in 1997 and in 2002. It can be seen from Figure 4 that the $\sigma_1 = 32.1$ isopycnal nearly surfaces above the EGC, and the northward transport in the MOC_σ mostly includes the NAC. Thus MOC_σ is representative of the water mass transformation occurring north of the section.

We notice that MOC_σ is stronger than the DWBC by about 7.5 Sv for both years. This difference can be explained by the export of some EGC water (mainly Irminger Sea Water and uLSW) from the Irminger Sea. Part of this water circulates cyclonically around the Labrador Sea before merging with the Labrador Current and being exported above the DWBC; a significant part enters the Labrador Sea (via eddies) and is transformed by isopycnal mixing or incorporated in the process of LSW formation. The fact that Ovide and Fourx MOC_σ values are so close to the MOC_z values at lower latitudes [*Koltermann et al.*, 1999; *Bryden et al.*, 2005] leads us to believe that the EGC water exported westward with a density above $\sigma_1 = 32.1$ belongs to the lower branch of the MOC at lower latitudes, either by deepening of the isopycnals south of the Labrador Gyre or by diapycnal mixing inside the gyre. Future studies will help to validate and develop this thesis.

6.4. MOC Strength, Heat and Freshwater Transport

Table 5. Comparison between 1997 and 2002 integrated transports. The MOC is calculated in z coordinates as the maximum of the transport accumulated over the whole section from surface to bottom (the shallower shaded area on Figure 15), and as the difference of its extrema (the intermediate shaded area on Figure 15). The MOC_σ is calculated as the maximum of the cumulative transport, but in σ coordinates (16). "Net transp." refers to the net volume transport in the inverse model. Errors are given by the inverse models, and don't take into account sources of errors like the asynopticity and the ageostrophic variability along the section but include EGCC sampling error (see section 4.1).

	1997 _{ADCP}	2002 _{Ssadcp}	Units
MOC_z/NAC	13.2 ± 0.9	8.8 ± 0.9	$10^6 \text{ m}^3 \text{ s}^{-1}$
$MOC_z/NADW$	14.2 ± 0.8	11.2 ± 0.8	$10^6 \text{ m}^3 \text{ s}^{-1}$
MOC_σ	19.2 ± 0.8	16.9 ± 1.0	$10^6 \text{ m}^3 \text{ s}^{-1}$
Net transp.	0.12	0.26	$10^6 \text{ m}^3 \text{ s}^{-1}$
Heat	0.66 ± 0.04	0.44 ± 0.05	10^{15} W
Salinity	15.2 ± 4.3	8.2 ± 4.4	10^9 kg s^{-1}

By performing different inversions, using or not LADCP, SADCP, and applying various constraints, we found that the MOC_z was actually quite sensitive to changes in the constraints, whereas the MOC_σ was much more stable. For example, MOC_z varies from 17 Sv to 14.2 Sv between A04 and the 1997 ADCP inversion, while MOC_σ varies only from 19 to 19.2 Sv . Similarly, comparing $Ssadcp$ and $Sgeost$ inversion in 2002 (with and without ADCP data), MOC_z differs by 4.3 Sv while MOC_σ differs by only 0.1 Sv .

Table 5 gives a summary of the different values for estimates of MOC strength and for heat and salt transport. The error is a result of the inversion, and in 2002, 0.7 Sv associated with the EGCC has been incorporated (see section 4.1).

Values of 14.2 Sv in 1997 and 11.2 Sv in 2002 are obtained for MOC_z/NADW in Table 5; but the MOC_z/NAC strength calculated as the peak in the transport accumulated from the surface represents 13.2 and 8.8 Sv respectively. Why are MOC_z/NADW and MOC_z/NAC so different? We observe a 2002 AABW net transport of 1.5 ± 1.1 Sv northward, twice as strong as in 1997 according to the new ADCP inversion. This strong flow participates in the difference between the two MOC definitions through the overall mass conservation, and is associated with the transformation of upwelled AABW in NADW north of the section.

This discussion leads us to consider that the MOC strength calculated in σ coordinates is a better proxy for the MOC than estimates calculated over z coordinates, as stated by *Marsh et al.* [2005]. With uncertainties based on one-standard-deviation range, we find that the MOC amplitude in June-July 2002 was significantly lower than in August 1997, with a decrease of 2.4 ± 1.8 Sv (about 15%). The maximum of the northward transport was obtained at $\sigma_1 = 32.1$, which lies at about 1000m within the NAC.

The heat transport is equal to 0.44 ± 0.05 PW (1 PW = 10^{15} W) in 2002, while it reached 0.66 ± 0.04 PW in 1997, which corresponds to a difference of about 30%.

The salinity flux is calculated assuming a strict zero mass flux as in *Bacon* [1997], obtained by imposing a mass conservation error of $0.1 \cdot 10^9$ kg s⁻¹. We find 8.2 ± 4.4 Sv psu northward in 2002, against 15.2 ± 4.3 in 1997 (Table 5). The errors include the possible omission of 0.7 Sv at 31 psu in the EGCC in 2002. The variability, although not significant, is consistent with the heat flux, reminding that the NAC is the main heat and salt source across the section. The Ovide 2002 value is similar to Bacon's 6.5 ± 2.2 Sv psu in 1991.

7. Discussion and Conclusion

The question arises whether the slightly different paths and seasons of Fourex and Ovide could explain some of the observed variability in the MOC strength. Although many qualitative issues were discussed in section 6.2, the net impact of the observed differences is difficult to quantify without the help of models. That is why this issue was thoroughly discussed in *Treguier et al.* [2006], using the eddy-resolving CLIPPER ATL6 and FLAME models for the 1995-2002 period. The models consistently show larger values of MOC _{σ} by 1-2 Sv across Fourex line than Ovide in all seasons, whereas the models present a 2 to 4 Sv decrease between Fourex 1997 and Ovide 2002. This is quite consistent with the data, and suggest that the observed difference in MOC _{σ}

is mostly time variability and not space variability. The differences are enhanced in depth coordinates, but they may also be less reliable, as discussed before.

Treguier et al. [2006] also showed that the orientation of the section allowed us to safely ignore the unresolved eddy contribution to the heat transport across the Ovide section. The difference in heat transport is remarkable (0.66 PW in August 1997 versus 0.44 PW in June 2002), but there again, the southern localisation of the Fourex line could be partly responsible, since the sections, although not zonal, lie on the steep slope of the zonally averaged heat transport [see *Ganachaud and Wunsch*, 2003, Figure 3]. To verify this potential contribution, the yearly-averaged surface heat flux between Ovide and Fourex sections was estimated as 0.02 PW, which indicates that the different paths of the sections are not responsible for the observed difference in heat transport. What about the monthly variability? The CLIPPER model run from *Treguier et al.* [2006] shows that the heat transport across Ovide section has the smallest variability in summer, and the difference estimated between June and August averaged on years 1995 to 2002 in the model gives -0.02 PW, with a standard deviation of 0.05 PW. Based on these model results, the difference in time and location of Ovide and Fourex sections would explain at most one third of the contrast observed between 1997 and 2002. This suggests that the observed heat transport variability is mainly a direct result of the MOC _{σ} variability between August 1997 and June-July 2002.

What about non-synopticity issues? The Ovide section was performed in 22 days. According to *Ganachaud* [2003], the uncertainty linked to the asynopticity is weak compared to those associated with geostrophic assumptions. Although these sources of error were included in the overall mass constraint, it has little effect on the resulting MOC error since the constraints from velocity measurements appear to have greater weight. Should we arbitrarily set the resulting MOC error to 3 Sv? We believe not; but we must emphasize that the present results are only one point representative of three weeks of the years 1997 and 2002, and considering the important month-to-month variability of this kind of indicator [*Wunsch and Heimbach*, 2006], conclusions on interannual variability should be drawn with the support of other studies.

In conclusion, it has been shown that the Ovide line is quite suitable to monitor the many circulation patterns of the North Atlantic circulation, including the Subpolar Gyre, the DWBC and the NAC. In the eastern Subpolar Gyre, the circulation is characterized by a strong East Greenland Current of nearly 27.7 Sv in 1997, compared to 22.4 Sv in 2002. In 1997, the northerly boundary of the NAC and the strong northward flow of LSW nearly reverse the flow at depth in CGFZ. In 2002, the NAC net transport is marked by a strong southward recirculation of warm surface water over the Iberian

Abyssal Plain, on top of a 2.2 Sv northward flow of AABW.

Besides these circulation patterns, we saw that the maximum of the transport integrated over the section from the surface along σ_1 coordinates is a good proxy for monitoring the North Atlantic Meridional Overturning Cell. Relying on this proxy, we show a 2.4 ± 1.8 Sv decrease of the MOC between Summer 1997 and Summer 2002, half of it being probably due to the different section paths. The heat transport sees an even more severe decrease of about 30%.

Acknowledgments.

The authors want to acknowledge the colleagues and ship crews who helped to collect all the data discussed in this paper. They are also grateful to Gilles Reverdin and an anonymous reviewer for their helpful and very detailed comments on the text that helped greatly to improve its precision and clarity. Figure 12 comes directly from the AVISO Live Access Server. For this work, P. Lherminier and C. Kermabon were supported by Ifremer, H. Mercier by CNRS, C. Gourcuff by Ifremer and CNES, and S. Bacon by NOCS. The Ovide project mainly relies on funds from Ifremer, INSU and PNEDC.

References

- Álvarez, M., H. L. Bryden, F. F. Pérez, A. F. Ríos, and G. Rosón (2002), Physical and biochemical fluxes and net budgets in the Subpolar and Temperate North Atlantic, *J. Mar. Res.*, *60*, 191–262.
- Álvarez, M., F. F. Pérez, H. L. Bryden, and A. F. Ríos (2004), Physical and biochemical transports structure in the North Atlantic subpolar gyre, *J. Geophys. Res.*, *109*, C03027, doi:10.1029/2003JC002015.
- Bacon, S. (1997), Circulation and fluxes in the North Atlantic between Greenland and Ireland, *J. Phys. Oceanogr.*, *27*, 1420–1435.
- Bacon, S. (1998a), Decadal variability in the outflow from the Nordic seas to the deep Atlantic Ocean, *Nature*, *394*, 871–874.
- Bacon, S. (1998b), RRS DISCOVERY Cruise 230: 07 Aug - 17 Sep 1997, *Tech. Rep. 16*, Southampton Oceanography Centre.
- Bacon, S., G. Reverdin, I. G. Rigor, and H. M. Snaith (2002), A freshwater jet on the east Greenland Shelf, *J. Geophys. Res.*, *107*, doi:10.1029/2001JC000935.
- Bacon, S., W. J. Gould, and Y. Jia (2003), Open-ocean convection in the Irminger Sea, *Geophys. Res. Lett.*, *30*(5), 1246, doi:10.1029/2002GL016271.
- Belkin, I. M., and S. Levitus (1996), Temporal variability of the subarctic front near the Charlie-Gibbs Fracture Zone, *J. Geophys. Res.*, *101*(C12), 28,317–28,324, doi:10.1029/96JC02794.
- Bersch, M. (2002), North Atlantic Oscillation-induced changes of the upper layer circulation in the northern North Atlantic Ocean, *J. Geophys. Res.*, *107*(C10), 3156, doi:10.1029/2001JC000901.
- Billant, A., P. Branell, and H. Mercier (2004), Campagne OVIDE 2002: rapport de données CTD-O₂, *Tech. Rep. DRO/DOPS/LPO/04-01*, Ifremer.
- Bryden, H. L., H. R. Longworth, and S. A. Cunningham (2005), Atlantic meridional overturning circulation at 25°N, *Nature*, *438*, 655–657, doi:10.1038/nature04385.
- Cunningham, S. A. (2000), Circulation and VOLUME flux of the North Atlantic using synoptic hydrographic data in a Bernoulli inverse, *J. Mar. Res.*, *58*, 1–35.
- Cuny, J., P. B. Rhines, and R. Kwok (2005), Davis Strait volume, freshwater and heat fluxes, *Deep-Sea Res.*, *52*, 519–542.
- Curry, R. G., and M. S. McCartney (2001), Ocean gyre circulation changes associated with the north atlantic oscillation, *J. Phys. Oceanogr.*, *31*, 3374–3400.
- Dickson, R. R., and J. Brown (1994), The production of North Atlantic Deep Water: sources, rates, and pathways, *J. Geophys. Res.*, *99*(C6), 12,319–12,341.
- Dickson, R. R., I. Yashayaev, J. Meincke, B. Turrell, S. Dye, and J. Holfort (2002), Rapid freshening of the deep North Atlantic Ocean over the past four decades, *Nature*, *416*, 832–837.
- Egbert, G., A. Bennett, and M. Foreman (1994), TOPEX/Poseidon tides estimated using a global inverse model, *J. Geophys. Res.*, *99*(C12), 24,821–24,852.
- Flatau, M. K., L. Talley, and P. P. Niiler (2003), The North Atlantic oscillation, surface current velocities, and SST changes in the subpolar North Atlantic, *J. Climate*, *16*, 2355–2369.
- Forner, S. (2005), Utilisation des CFC et du CCl₄ dans l'étude de la circulation profonde de l'Atlantique Nord, Ph.D. thesis, Université de Bretagne Occidentale.
- Fratantoni, D. M. (2001), North Atlantic surface circulation during the 1990s observed with satellite-tracked drifters, *J. Geophys. Res.*, *106*(C10), 22,067–22,094, doi:10.1029/2000JC000730.
- Ganachaud, A. (2003), Error budget of inverse box models: the North Atlantic, *J. Atmos. Ocean. Technol.*, *20*(11), 1641–1655.
- Ganachaud, A., and C. Wunsch (2003), Large-scale ocean heat and freshwater transports during the World Ocean Circulation Experiment, *J. Climate*, *16*(2), 696–705.
- Häkkinen, S., and P. B. Rhines (2004), Decline of subpolar North Atlantic, *Science*, *304*, 555–559.
- Hansen, B., and S. Østerhus (2006), Monitoring the Faroe Bank Channel overflow, Geophysical Research Abstracts, Vol. 8, 06841, 2006.
- Harvey, J. G., and A. Theodorou (1986), The circulation of Norwegian Sea overflow water in the eastern North Atlantic, *Oceanologica Acta*, *9*(4), 393–402.
- Hátún, H., A. B. Sandø, H. Drange, B. Hansen, and H. Valdimarsson (2005), Influence of the Atlantic Subpolar Gyre on the thermohaline circulation, *Science*, *309*, 1841–1844, doi:10.1126/science.1114777.
- Koltermann, K. P., A. V. Sokov, V. P. Tereschenkov, S. A. Dobroliubov, K. Lorbacher, and A. Sy (1999), Decadal changes in the thermohaline circulation of the North Atlantic circulation during the 1990s, *Science*, *286*, 109–138.
- Kraus, W. (1995), Currents and mixing in the Irminger Sea and in the Iceland Basin, *J. Geophys. Res.*, *100*(C6), 10,851–10,871.
- Lavender, K. L., R. E. Davis, and W. B. Owens (2000), Mid-depth recirculation observed in the interior Labrador and Irminger seas by direct velocity measurements, *Nature*, *407*, 66–69.
- Lherminier, P., J.-P. Gouillou, C. Kermabon, and H. Mercier (2003), OVIDE 2002: traitement des données des LADCP RDI-BB150 et RDI-WH300, *Tech. Rep. DRO/DOPS/LPO/03-10*, Ifremer.
- Lux, M., H. Mercier, and M. Arhan (2000), Interhemispheric exchanges of mass and heat in the Atlantic Ocean in January-March 1993, *Deep-Sea Res.*, *48*, 605–638.
- Macrander, A., U. Send, H. Valdimarsson, S. Jonsson, and R. H. Käse (2005), Interannual changes in the overflows from the Nordic Seas into the Atlantic Ocean through Denmark Strait, *Geophys. Res. Lett.*, *32*(L06606), doi:10.1029/2004GL021463.
- Marsh, R., B. A. de Cuevas, A. C. Coward, H. L. Bryden, and M. Alvarez (2005), Thermohaline circulation at three key sections in the North Atlantic over 1985–2002, *Geophys. Res. Lett.*, *32*(L10604), doi:10.1029/2004GL022281.
- Maslowski, W., D. Marble, W. Walczowski, U. Schauer, J. L. Clement, and A. J. Semtner (2004), On climatological mass, heat and salt transports through the Barents Sea and Fram Strait from a pan-Arctic coupled ice-ocean model simulation, *J. Geophys. Res.*, *109*(C3), C03,032, doi:10.1029/2001JC001039.
- McCartney, M. S. (1992), Recirculating components to the deep boundary current of the northern North Atlantic, *Prog. Oceanogr.*, *29*(4), 283–383.
- Mercier, H. (1986), Determining the General Circulation of the Ocean: A Non Linear Inverse Problem, *J. Geophys. Res.*, *91*(C4), 5103–5109.
- Paillet, J., and H. Mercier (1997), An inverse model of the eastern North Atlantic general circulation and thermocline ventilation, *Deep-Sea Res.*, *44*(8), 1293–1328.
- Paillet, J., M. Arhan, and M. S. McCartney (1998), Spreading of Labrador Sea Water in the eastern North Atlantic, *J. Geophys. Res.*, *103*(C5), 10,223–10,239.
- Pickart, R. S., F. Straneo, and G. W. K. Moore (2003), Is Labrador Sea Water formed in the Irminger basin?, *Deep-Sea Res.*, *50*(1), 23–52.

- Pickart, R. S., D. J. Torres, and P. S. Fratantoni (2005), The East Greenland Spill Jet, *J. Phys. Oceanogr.*, *35*(6), 1037–1053, doi:10.1175/JPO2734.1.
- Reverdin, G., P. P. Niiler, and H. Valdimarsson (2003), North Atlantic Ocean surface currents, *J. Geophys. Res.*, *108*, doi:10.1028/2001JC001020.
- Saunders, P. M. (1987), Flow through Discovery Gap, *J. Phys. Oceanogr.*, pp. 631–643.
- Saunders, P. M. (1994), The flux of overflow water through the Charlie Gibbs Fracture Zone, *J. Geophys. Res.*, *99*, 12,343–12,355.
- Schmitz, W. J., Jr., and M. S. McCartney (1993), On the North Atlantic circulation, *Reviews of Geophysics*, *31*(1), 29–49.
- Schott, F., L. Stramma, and J. Fischer (1999), Interaction of the North Atlantic Current with the deep Charlie Gibbs Fracture Zone throughflow, *Geophys. Res. Lett.*, *26*, 369–372.
- Serreze, M. C., A. P. Barrett, A. G. Slater, R. A. Woodgate, K. Aagaard, R. B. Lammers, M. Steele, R. Moritz, M. Meredith, and C. M. Lee (2006), , *J. Geophys. Res.*, *111*(C11010), doi:10.1029/2005JC003424.
- Sy, A. (1988), Investigation of large-scale circulation patterns in the central North Atlantic Current, the Azores Current, and the Mediterranean Water plume in the area of the Mid-Atlantic Ridge, *Deep-Sea Res.*, *35*, 383–413.
- Treguier, A.-M., S. Theetten, E. Chassignet, T. Penduff, R. Smith, L. Talley, J. O. Beismann, and C. Böning (2005), The North Atlantic subpolar gyre in four high-resolution models, *J. Phys. Oceanogr.*, *35*(5), 757–774, doi:10.1175/JPO2720.1.
- Treguier, A.-M., C. Gourcuff, P. Lherminier, H. Mercier, B. Barnier, G. Madec, J. Molines, T. Penduff, L. Czeschel, and C. Böning (2006), Internal and forced variability along a section between Greenland and Portugal in the CLIPPER Atlantic model, *Oceans Dynamics*, doi:10.1007/s10236-006-0069-y.
- Uppala, S., P. Kallberg, A. Simmons, U. Andrae, V. da Costa Bechtold, M. Fiorino, J. Gibson, J. Haseler, A. Hernandez, G. Kelly, X. Li, K. Onogi, S. Saarinen, N. Sokka, R. Allan, E. Andersson, K. Arpe, M. Balmaseda, A. Beljaars, L. van de Berg, J. Bidlot, N. Bormann, S. Caires, F. Chevallier, A. Dethof, M. Dragosavac, M. Fisher, M. Fuentes, S. Hagemann, E. Holm, B. Hoskins, L. Isaksen, P. Janssen, R. Jenne, A. McNally, J.-F. Mahfouf, J.-J. Morcrette, N. Rayner, R. Saunders, P. Simon, A. Sterl, K. Trenberth, A. Untch, D. Vasiljevic, P. Viterbo, and J. Woollen (2005), The ERA-40 re-analysis, *Quart. J. Roy. Meteor. Soc.*, *131*, 2961–3012.
- van Aken, H. M., and G. Becker (1996), Hydrography and through-flow in the north-eastern North Atlantic Ocean: the NANSEN project, *Prog. Oceanogr.*, *38*(4), 297–346, doi:10.1016/S0079-6611(97)00005-0.
- Visbeck, M. (2002), Deep velocity profiling using Lowered Acoustic Doppler Current Profilers: bottom track and inverse solutions, *J. Atmos. Ocean. Technol.*, *19*(5), 794–807.
- Wilkinson, D., and S. Bacon (2005), The spatial and temporal variability of the East Greenland Coastal Current from historic data, *Geophys. Res. Lett.*, *submitted*.
- Woodgate, R. A., and K. Aagaard (2005), Revising the bering strait freshwater flux into the arctic ocean, *Geophys. Res. Lett.*, *32*(L02602), doi:10.1029/2004GL021747.
- Wunsch, C., and P. Heimbach (2006), Estimated decadal changes in the North Atlantic Meridional Overturning Circulation and heat flux 1993-2004, *J. Phys. Oceanogr.*, *36*(11), 2012–2024, doi:10.1175/JPO2957.1.
- Yashayaev, I., and A. Clarke (2005), Recent warming of the Labrador Sea, ASOF Newsletter No. 4, p.17-18 (unpublished manuscript).

P. Lherminier, Laboratoire de Physique des Océans, Ifremer, B.P. 70, 29280 PLOUZANE, FRANCE. (pascale.lherminier@ifremer.fr)